J. Fluid Mech. (1989), *vol.* 205, *pp.* 359–396
Printed in Great Britain

Lubricated pipelining: stability of core–annular flow. Part 2

By HOWARD H. HU AND DANIEL D. JOSEPH
Department of Aerospace Engineering and Mechanics, University of Minnesota, Minneapolis, MN 55455, USA

(Received 12 April 1988 and in revised form 5 January 1989)

In this paper, we study the linearized stability of three symmetric arrangements of two liquids in core–annular Poiseuille flow in round pipes. Deferring to one important application, we say oil and water when we mean more viscous and less viscous liquids. The three arrangements are (i) oil is in the core and water on the wall, (ii) water is in the core and oil is outside and (iii) three layers, oil inside and outside with water in between. The arrangement in (iii) is our model for lubricated pipelining when the pipe walls are hydrophobic and it has not been studied before. The arrangement in (ii) was studied by Hickox (1971) who treated the problem as a perturbation of long waves, effectively suppressing surface tension and other essential effects which are necessary to explain the flows observed, say, in recent experiments of W. L. Olbricht and R. W. Aul. The arrangement in (i) was studied in Part 1 of this paper (Preziosi, Chen & Joseph 1987). We have confirmed and extended their pseudo-spectral calculation by introducing a more efficient finite-element code. We have calculated neutral curves, growth rates, maximum growth rate, wavenumbers for maximum growth and the various terms which enter into the analysis of the equation for the evolution of the energy of a small disturbance. The energy analysis allows us to identify the three competing mechanisms underway: interfacial tension, interfacial friction and Reynolds stress. Many results are presented.

1. Introduction

This paper extends the work of Joseph, Renardy & Renardy (1984) and of Preziosi, Chen & Joseph (1989, hereinafter referred to as PCJ) on the stability of core–annular flow of two liquids in a pipe. The introduction of PCJ emphasized applications to lubricated pipelining and reviewed the place such studies take in the dynamics of flow of two fluids. The introduction given there serves well here. As in PCJ, we consider the problem of linearized stability of core–annular flows of two liquids with different densities and viscosities with surface tension included but gravity excluded. Going beyond PCJ, we have treated the problem with a water core and oil on the wall, studied previously by Hickox (1971) for long waves, for all wavenumbers and Reynolds numbers, with effects of surface tension included. The extended analysis of this problem appears to be in good agreement with new experiments of W. L. Olbricht and R. W. Aul (private communication) on water flow in an oil coated glass tube of small (54 μm) diameter. The applications of such experiments were more related to problems of oil recovery than to lubricated pipelining. We also studied the problem of lubricated flow of viscous liquid when a layer of viscous fluid coats the pipe wall, modelling the situation in lubricated pipelining of oil when the pipe walls

are hydrophobic. In this case, the pipe wall takes on oil, but the oil core is lubricated by water in a layer between the core and the oil coating the wall.

PCJ identified a window of parameters in which core–annular flow was stable to small disturbances. For stability, the water fraction cannot be too large, about 40% at most, and the Reynolds number for the core rests in a range $\mathbb{R}_L < \mathbb{R} < \mathbb{R}_U$ where $\mathbb{R}_L$ is the lower critical value below which core–annular flow is unstable to capillary forces and $\mathbb{R}_U$ is the upper critical value. PCJ compared their results with the experiments of Charles, Govier & Hodgson (1961), and they noticed that the cases of instability with $\mathbb{R} > \mathbb{R}_U$ were correlated with the emulsification of water into oil.

Most of the cases studied by PCJ and all of the new ones studied here are unstable. The utility of linear theory for understanding unstable flow is problematic, since the flows that arise from instability are a perturbation of core–annular flow only in some special circumstances involving stable bifurcation. The flows that actually arise from instability in practice seem in general not to be close to core–annular flow.

To use linearized stability theory to understand unstable flow it is necessary to be guided by experiments. The experiments relevant to lubricated pipelining are listed in PCJ. Of these, the experiments of Charles *et al.* (1961) are best for comparing, because they eliminated gravity by matching the density of water with a mixture of oil and carbon tetrachloride. The effects of gravity are not so serious as to destroy lubricated pipelining (Oliemans & Ooms 1986). Some observations about the effects of gravity are mentioned by PCJ.

Hasson, Mann & Nir (1970) and Hasson & Nir (1970) studied the problem of core–annular flow with water inside $(\rho, \mu) = (1\ \text{g/cc},\ 0.82\ \text{cP})$ and an organic liquid $(\rho, \mu) = (1.02\ \text{g/cc},\ 1\ \text{cP})$ outside. The core–annular arrangement was always unstable. W. L. Olbricht and R. W. Aul are at present carrying out experiments in a manner that gives data suitable for comparison with theory. These experiments are discussed in detail in §8.3.

We are doing our own experiments, but the results are too preliminary for a systematic account. Three observations are important. We are able to achieve a wonderful lubrication of a coal–oil dispersion (40% in SAE 30 motor oil) in water. The dispersion is very nearly density matched; and it could not be economically transported in a pipe without water because, at this high concentration of coal, the dispersion is a plastic fluid with an enormous viscosity. We also get a lubricated flow in three layers in glass pipes which are hydrophobic. The third observation is that we always see waves on thin oil films wetting glass when there is a shear driven by water. We shall argue that these waves are driven by interfacial friction associated with the viscosity difference. Linear theory shows that these waves are unstable; perhaps they are equilibrated by nonlinear effects (cf. Oliemans & Ooms 1986; Frenkel *et al.* 1987). The waves we see on thin layers of oil driven by the shear flows of water are reminiscent of water waves generated by wind. This problem was studied by Blennerhassett (1980) from the point of view of nonlinear stability theory. Of course, unstable interfacial waves driven by interfacial friction can be equilibrated by effects of gravity when the dense fluid is below, as in water waves driven by the wind. Travelling waves can be expected to arise from instability and birurcation of stable core–annular flows (Renardy & Joseph 1986). The waves determined by the impressive computation of Blennerhassett (1980) do not seem to fit the experimental data for water waves well, but we think this line of inquiry should not be closed.

A list of hydrodynamical structures which can be imagined to arise from the instability of core–annular flow are: (*a*) bubbles and slugs of oil in water; (*b*) drops of water in oil; (*c*) emulsions, mainly of water in oil; (*d*) wavy interfaces. Of these, it

would seem that only some of the wavy interfaces could be regarded as arising out of stable bifurcation of core–annular flow. We might hope for a good agreement between the linear theory and experiments for this case.

In the cases (*a*, *b*, *c*) mentioned above, the comparison between linear theory and experiments is more problematic. We have basically three procedures which can be used.

(1) We can compute maximum growth rates and the wavelength of the fastest growing wave. This length can be compared with the size of bubbles and slugs which arise in experiments. The agreements between the calculations of PCJ and experiments of Charles *et al.* (1961) were rather better than what one might have expected.

(2) We can calculate neutral curves and try to compare regions of parameter space in the stability diagrams with the corresponding regions in experiments. This procedure is global in parameters and it appears to be promising.

(3) We can compute various terms that arise in the global balance of energy of a small disturbance. This type of computation was introduced by Hooper & Boyd (1983, 1987), and it is particularly useful in the present context. We can identify different instabilities. We obtain integrated Reynold stresses in the bulk fluid, as in the case of one fluid; but when there are two fluids, we can compare the contributions to the total made by each of the fluids. We obtain boundary terms, one proportional to interfacial tension, another to interfacial friction (proportional to the viscosity difference), and each of these contributions appears on every interface. All these terms take positive and negative values as the parameters are varied, and they compete to determine whether the average energy of a disturbance will increase or decrease. For now, it will suffice to note that interfacial tension is always dominant and always destabilizing at the smallest Reynolds numbers. Interfacial friction can stabilize interfacial tension (capillary instability) and, in fact, is a major actor in the stabilization of core–annular flow with oil cores. In other circumstances, interfacial friction destabilizes and it always destabilizes flow with water cores when the walls are wet by oil. The Reynolds stress in the core is not destabilizing; water cores are never destabilized by Reynolds stress. The Reynolds stress contribution in the water annulus lubricating the core will always lead to instability, whether or not water or oil is on the wall.

For all of the results in this paper, we used a finite-element code which runs efficiently even for small values, less than 10^{-4}, of the ratio of viscosity of water to oil where the problem is known to become singular. Only a sample from the library of results, which could be generated by five or even six independent parameters, will be presented here. The reader will find a more complete enumeration of results in the conclusion of the paper.

2. The basic flow

Consider the problem of two liquids flowing down a circular pipe in three layers with the inner and outer layer occupied by liquid 1 and middle layer by liquid 2. The interfaces between liquids are $r = r_1(\theta, z, t)$ and $r = r_2(\theta, z, t)$, $(r_2 > r_1)$, where (r, θ, z) are cylindrical coordinates and t is time. Let $\boldsymbol{U} = (u_r, u_\theta, u_z)$ be velocity and $\hat{p}$ be pressure, μ_1, ρ_1 be the viscosity and density of liquid 1, μ_2 and ρ_2 of liquid 2.

Assume that the pipe is infinitely long with radius R_3 and axis at $r = 0$, the mean value of r_1 (and r_2) over $\theta (0 \leqslant \theta \leqslant 2\pi)$ is R_1 (and R_2), a constant independent of time, and the gravity force can be neglected.

We scale the length with R_3, velocity with the centreline velocity of the basic flow W_0, pressure with $\rho_1 W_0^2$, time with R_3/W_0 and use the same symbols for dimensional and dimensionless variables.

The basic core–annular flow with constant pressure gradient $\partial P/\partial z = -F$ is

$$\boldsymbol{U} = (0, 0, W(r)), \tag{2.1}$$

with

$$W(r) = \begin{cases} [(b^2-\eta^2)+m(1+\eta^2-b^2-r^2)]/A, & r\in[0,\eta], \\ [b^2-r^2+m(1-b^2)]/A, & r\in[\eta,b], \\ [m(1-r^2)]/A, & r\in[b,1], \end{cases} \tag{2.2}$$

where

$$W_0 = \frac{F}{4\mu_2}[m(R_1^2+R_3^2-R_2^2)+R_2^2-R_1^2], \tag{2.3}$$

$$A = b^2-\eta^2+m(1+\eta^2-b^2), \tag{2.4}$$

and

$$m = \frac{\mu_2}{\mu_1}, \quad \eta = \frac{R_1}{R_3}, \quad b = \frac{R_2}{R_3}. \tag{2.5}$$

3. Perturbation equations and normal mode

We perturb the core–annular flow with

$$\boldsymbol{U} = (u, v, w+W), \quad \hat{p} = P+p, \quad r_l = \eta \text{ (or } b) + \delta_l(\theta, z, t) \quad (l = 1, 2) \tag{3.1}$$

and introduce dimensionless parameters

$$\zeta = \frac{\rho_2}{\rho_1}, \quad \mathbb{R} = \frac{\rho_1 W_0 R_3}{\mu_1}, \quad J^* = \frac{TR_3\rho_1}{\mu_1^2}. \tag{3.2}$$

Using the normal-mode decomposition of solutions:

$$\left.\begin{aligned} [u, v, w, p](r, \theta, z, t) &= [\mathrm{i}u, v, w, p](r)\exp[in\theta+\mathrm{i}\beta(z-ct)] \\ \text{and} \qquad [\delta_1, \delta_2](\theta, z, t) &= [\delta_1, \delta_2]\exp[in\theta+\mathrm{i}\beta(z-ct)], \end{aligned}\right\} \tag{3.3}$$

where $u(r), v(r), w(r), p(r)$ are complex-valued functions, and δ_1, δ_2 are complex constants. If we write $\delta_1 = |\delta_1|\mathrm{e}^{\mathrm{i}\phi_1}, \delta_2 = |\delta_2|\mathrm{e}^{\mathrm{i}\phi_2}$, then $\phi_2-\phi_1$ indicates the phase shift of two interfaces in the z-direction.

The linearized equations of motion are

$$\zeta_l\beta(W-c)u = p' - \frac{\mathrm{i}m_l}{\mathbb{R}}\left[\frac{\mathrm{d}}{\mathrm{d}r}\left(\frac{\mathrm{d}ru}{r\,\mathrm{d}r}\right)-\left(\beta^2+\frac{n^2}{r^2}\right)u-\frac{2n}{r^2}v\right], \tag{3.4}$$

$$\zeta_l\beta(W-c)v = -\frac{n}{r}p - \frac{\mathrm{i}m_l}{\mathbb{R}}\left[\frac{\mathrm{d}}{\mathrm{d}r}\left(\frac{\mathrm{d}rv}{r\,\mathrm{d}r}\right)-\left(\beta^2+\frac{n^2}{r^2}\right)v-\frac{2n}{r^2}u\right], \tag{3.5}$$

$$\zeta_l[\beta(W-c)w+W'u] = -\beta p - \frac{\mathrm{i}m_l}{\mathbb{R}}\left[\frac{1}{r}\frac{\mathrm{d}}{\mathrm{d}r}\left(r\frac{\mathrm{d}w}{\mathrm{d}r}\right)-\left(\beta^2+\frac{n^2}{r^2}\right)w\right], \tag{3.6}$$

$$\frac{\mathrm{d}ru}{r\,\mathrm{d}r}+\frac{n}{r}v+\beta w = 0, \tag{3.7}$$

where $W' = \mathrm{d}W/\mathrm{d}r$, $m_l = (1, m, 1)$, $\zeta_l = (1, \zeta, 1), l = 1, 2, 3$ indicates the flow region $\Omega_1 = [0, \eta), \Omega_2 = (\eta, b), \Omega_3 = (b, 1]$ with $\rho_3 = \rho_1$ and $\mu_3 = \mu_1$.

The boundary conditions are

$$r = 1: \quad u = v = w = 0, \tag{3.8}$$

$$r = 0: \quad u, v, w, p \quad \text{and their derivatives are finite}, \tag{3.9}$$

and the linearized interface conditions are $r = \eta$ and b (corresponds to $l = 1, 2$):

$$u(r_l) = \beta(W-c)\,\delta_l, \tag{3.10}$$

$$[\![u]\!]_l = [\![v]\!]_l = 0, \tag{3.11}$$

$$[\![w]\!]_l + [\![W']\!]_l\,\delta_l = 0, \tag{3.12}$$

$$[\![m_l(-\beta u + w')]\!]_l = 0, \tag{3.13}$$

$$\left[\!\!\left[m_l\left(-\frac{nu+v}{r} + v'\right)\right]\!\!\right]_l = 0, \tag{3.14}$$

$$[\![p]\!]_l - \frac{2\mathrm{i}}{\mathbb{R}}[\![m_l u']\!]_l = -\frac{J^*}{\mathbb{R}^2}\frac{1}{r_l^2}(1-n^2-r_l^2\beta^2)\,\delta_l, \tag{3.15}$$

where for any function $G(r)$ in $\Omega = \Omega_1 \cup \Omega_2 \cup \Omega_3$, $[\![m_l G]\!]_l$ is defined as

$$[\![m_l G]\!]_l = m_l G(r_l^-) - m_{l+1} G(r_l^+).$$

We could eliminate δ_l in (3.12) and (3.15):

$$u[\![W']\!]_l - (W-c)[\![u']\!]_l = 0, \tag{3.16}$$

$$[\![p]\!]_l - \frac{2\mathrm{i}}{\mathbb{R}}[\![m_l u']\!]_l = -\frac{J^*}{\mathbb{R}^2}\frac{1}{r_l^2}\frac{[\![u']\!]_l}{\beta[\![W']\!]_l}(1-n^2-r_l^2\beta^2). \tag{3.17}$$

4. Finite-element formulation

Define functional spaces

$$V = \{u, v \mid u \in c^1(\Omega), v \in c^0(\Omega); \quad \text{at } r = 1, u(1) = u'(1) = v(1) = 0;$$

$$\text{at } r = 0, u, v \quad \text{and their derivatives are finite};$$

$$\text{at } r = r_l, [\![u]\!]_l = [\![v]\!]_l = 0 \quad \text{and} \quad u[\![W']\!]_l - (W-c)[\![u']\!]_l = 0\}.$$

Thus, solving the equations (3.4)–(3.7) is equivalent to solving the following problem (weak solution):

Finding $u, v \in V$ for $\forall\, u^*, v^* \in V$, satisfying:

$$\begin{aligned}
&\sum_{l=1}^{3}\int_{\Omega_l}\zeta_l\left\{\left[\beta(W-c)uu^* + \frac{1}{\beta}(W-c)\frac{\mathrm{d}ru}{r\,\mathrm{d}r}\frac{\mathrm{d}ru^*}{r\,\mathrm{d}r} - \frac{W'}{\beta}u\frac{\mathrm{d}ru^*}{r\,\mathrm{d}r}\right] + \frac{n}{\beta}\left[\left(W-c\right)\frac{v}{r}\frac{\mathrm{d}ru^*}{r\,\mathrm{d}r}\right]\right\} r\,\mathrm{d}r \\
&= \frac{\mathrm{i}}{\mathbb{R}\beta^2}\sum_{l=1}^{3}\int_{\Omega_l} m_l\left\{\left[\frac{\mathrm{d}}{\mathrm{d}r}\left(\frac{\mathrm{d}ru}{r\,\mathrm{d}r}\right)\frac{\mathrm{d}}{\mathrm{d}r}\left(\frac{\mathrm{d}ru^*}{r\,\mathrm{d}r}\right) + \left(2\beta^2 + \frac{n^2}{r^2}\right)\frac{\mathrm{d}ru}{r\,\mathrm{d}r}\frac{\mathrm{d}ru^*}{r\,\mathrm{d}r} + \left(\beta^2 + \frac{n^2}{r^2}\right)\beta^2 uu^*\right]\right. \\
&\quad + n\left[\frac{\mathrm{d}}{\mathrm{d}r}\left(\frac{v}{r}\right)\frac{\mathrm{d}}{\mathrm{d}r}\left(\frac{\mathrm{d}ru^*}{r\,\mathrm{d}r}\right) + \left(\beta^2 + \frac{n^2}{r^2}\right)\frac{v}{r}\frac{\mathrm{d}ru^*}{r\,\mathrm{d}r} + \frac{2\beta^2}{r^2}vu^*\right]\Bigg\} r\,\mathrm{d}r \\
&\quad + \left[\left(p - \frac{\mathrm{i}m_l}{\mathbb{R}}\frac{\mathrm{d}ru}{r\,\mathrm{d}r}\right)ru^* + \frac{\mathrm{i}m_l}{\beta\mathbb{R}}w'\frac{\mathrm{d}ru^*}{r\,\mathrm{d}r}r\right]_{-0+\eta+b+1}
\end{aligned} \tag{4.1}$$

and

$$\sum_{l=1}^{3}\int_{\Omega_l}\zeta_l\left\{\frac{n}{\beta}\left[\left(W-c\right)\frac{\mathrm{d}ru}{r\,\mathrm{d}r}-W'u\right]\frac{v^*}{r}+\frac{1}{\beta}(W-c)\left(\beta^2+\frac{n^2}{r^2}\right)vv^*\right\}r\,\mathrm{d}r$$

$$=\frac{\mathrm{i}}{\mathbb{R}}\sum_{l=1}^{3}\int_{\Omega_l}m_l\left\{\frac{n}{\beta^2}\left[\frac{\mathrm{d}}{\mathrm{d}r}\left(\frac{\mathrm{d}ru}{r\,\mathrm{d}r}\right)\frac{\mathrm{d}}{\mathrm{d}r}\left(\frac{v^*}{r}\right)+\left(\beta^2+\frac{n^2}{r^2}\right)\frac{\mathrm{d}ru}{r\,\mathrm{d}r}\frac{v^*}{r}+\frac{2\beta^2}{r^2}uv^*\right]\right.$$

$$\left.+\left[\frac{\mathrm{d}rv}{r\,\mathrm{d}r}\frac{\mathrm{d}rv^*}{r\,\mathrm{d}r}+\frac{n^2}{\beta^2}\frac{\mathrm{d}}{\mathrm{d}r}\left(\frac{v}{r}\right)\frac{\mathrm{d}}{\mathrm{d}r}\left(\frac{v^*}{r}\right)+\left(\beta^2+\frac{n^2}{r^2}\right)\left(1+\frac{n^2}{\beta^2r^2}\right)vv^*\right]\right\}r\,\mathrm{d}r$$

$$+\left[\frac{\mathrm{i}m_l}{\mathbb{R}}\left(\frac{n}{r\beta}w'-\frac{\mathrm{d}rv}{r\,\mathrm{d}r}\right)rv^*\right]_{-0+\eta+b+1} \tag{4.2}$$

where $[\ldots]_{-0+\eta+b+1}=-[\ldots]_{r=0}+[\![\ldots]\!]_1+[\![\ldots]\!]_2+[\ldots]_{r=1}$.

Using the boundary conditions and interface conditions, we find two additional terms caused by interfaces and boundaries

$$\left[\left(p-\frac{\mathrm{i}m_l}{\mathbb{R}}\frac{\mathrm{d}ru}{r\,\mathrm{d}r}\right)ru^*+\frac{\mathrm{i}m_l}{\beta\mathbb{R}}w'\frac{\mathrm{d}ru}{\mathrm{d}r}\right]_{-0+\eta+b+1}$$

$$=\frac{\mathrm{i}}{\mathbb{R}}\{[\![m_l\,u']\!]_1\,\eta u^*(\eta)+(1-m)\,u(\eta)\,\eta u^{*\prime}(\eta)\}-\frac{J^*A}{2\beta\mathbb{R}^2}\frac{1-n^2-\eta^2\beta^2}{\eta^2(1-m)}[\![u']\!]_1\,u^*(\eta)$$

$$+\frac{\mathrm{i}}{\mathbb{R}}\{[\![m_l\,u']\!]_2\,bu^*(b)-(1-m)\,u(b)\,bu^{*\prime}(b)\}+\frac{J^*A}{2\beta\mathbb{R}^2}\frac{1-n^2-b^2\beta^2}{b^2(1-m)}[\![u']\!]_2\,u^*(b) \tag{4.3}$$

$$\left[\frac{\mathrm{i}m_l}{\mathbb{R}}\left(\frac{n}{r\beta}w'-\frac{\mathrm{d}rv}{r\,\mathrm{d}r}\right)rv^*\right]_{-0+\eta+b+1}$$

$$=\frac{\mathrm{i}}{\mathbb{R}}[u(0)-v(0)]\,v^*(0)-\left[2(1-m)\frac{\mathrm{i}}{\mathbb{R}}v(\eta)\,v^*(\eta)\right]+\left[2(1-m)\frac{\mathrm{i}}{\mathbb{R}}v(b)\,v^*(b)\right]. \tag{4.4}$$

In the finite-element method, the domain Ω is divided into simple geometric subdomains or elements; u, v are approximated in each element using values of u (and derivatives of u) and v at nodal points and interpolation functions. We take the piecewise cubic Hermite interpolation functions for u and the piecewise linear Lagrange interpolation functions for v, since the governing equation for u after eliminating w is fourth order while the equation for v is second order. Thus the unknowns at each node are $(u, \mathrm{d}u/\mathrm{d}r, v)$.

After discretization of (4.1) and (4.2), we could combine them into matrix form

$$\boldsymbol{A}\boldsymbol{x}=c\boldsymbol{B}\boldsymbol{x}. \tag{4.5}$$

where c is the eigenvalue in $(z-ct)$ in (3.3), $\boldsymbol{A}$ and $\boldsymbol{B}$ are the global matrices with the forced boundary conditions (3.8), (3.11) and (3.16) being applied, and $\boldsymbol{x}=[u_1, u_1', v_1, u_2', v_2, \ldots, u_N, u_N', v_N]^{\mathrm{T}}$, N is the total number of nodes.

Using the IMSL routine EIGZC, the eigenvalue $c=c_{\mathrm{r}}+\mathrm{i}c_{\mathrm{i}}$ of the problem (taken as the eigenvalue with the largest imaginary part c_{i}) and the corresponding eigenfunction are solved. If the computed eigenvalue $c_{\mathrm{i}}<0$, the perturbation will decay with time, and the flow is stable to this mode of perturbation. If $c_{\mathrm{i}}>0$, then, in linear stability theory, this mode of perturbation will grow exponentially with a growth rate of βc_{i}. This means the basic flow is unstable. Thus $c_{\mathrm{i}}=0$ indicates the neutral state.

5. Energy analysis

The energy method is useful in the analysis of the stability of the flow of one fluid because certain limited nonlinear results can be obtained from the method by elementary, yet rigorous, analysis. It is known that the utility of the method for the classical case of the flow of one fluid is basically restricted to the analysis of sufficient conditions for stability, though a recent approach of Galdi (1987) goes in another direction. The situation is greatly different for the case of two fluids. The main new feature is the appearance of new terms on the boundary. Hooper & Boyd (1983, 1987) and Hooper (1987) showed that the linearized energy equation can be used to analyse instability. When the energy equation solutions are evaluated, we may determine the situations in which instability is introduced through the Reynolds stress, as in one fluid, or in the boundary terms, through the surface tension and viscosity difference. There are three instabilities that may be identified through the energy: due to interfacial tension, interfacial friction and Reynolds stress. The analysis of the parameter dependence of these instabilities together with a comparison with experiments gives this type of analysis a potential for uncovering the basic dynamics of the flow that was never possible in the case of one fluid.

Mathematically, the energy analysis of the nonlinear stability of the flow of two fluids is frustrated by the fact that the boundary terms cannot be estimated *a priori* in terms of the dissipation (Joseph 1987).

After multiplying (3.4), (3.5) and (3.6) by u_*, v_* and w_*, the complex conjugates of u, v, w, we integrate and add the three equations using (3.7) and boundary conditions (3.8), (3.9) to obtain

$$\sum_{l=1}^{3}\int_{\Omega_l}\zeta_l[\beta(W-c)(u^2+v^2+w^2)+W'uw_*]\,r\,\mathrm{d}r$$

$$=\frac{\mathrm{i}}{\mathbb{R}}\sum_{l=1}^{3}\int_{\Omega_l}m_l\left[\left(\frac{\mathrm{d}ru}{r\,\mathrm{d}r}\right)^2+\left(\frac{\mathrm{d}rv}{r\,\mathrm{d}r}\right)^2+\left(\frac{\mathrm{d}w}{\mathrm{d}r}\right)^2+\left(\beta^2+\frac{n^2}{r^2}\right)(u^2+v^2+w^2)+\frac{4n}{r^2}uv_*\right]r\,\mathrm{d}r$$

$$+\left[\!\!\left[pru_*-\frac{\mathrm{i}}{\mathbb{R}}m_l\left(\frac{\mathrm{d}ru}{r\,\mathrm{d}r}ru_*+\frac{\mathrm{d}rv}{r\,\mathrm{d}r}rv_*+\frac{\mathrm{d}w}{\mathrm{d}r}rw_*\right)\right]\!\!\right]_{\eta+b}+\frac{\mathrm{i}}{\mathbb{R}}[u_{(0)}^2+v_{(0)}^2],\tag{5.1}$$

where $u^2=uu_*, v^2=vv_*, \ldots$. Each term in the equation is some kind of energy; thus (5.1) represents the energy balance for the perturbed flow. The imaginary part of (5.1) governs the growth of the energy of the small perturbations and it can be separated into four terms:

$$\dot{E}=I-D+B,\tag{5.2}$$

where

$$\dot{E}=\beta c_{\mathrm{i}}\sum_{l=1}^{3}\int_{\Omega_l}\zeta_l(u^2+v^2+w^2)\,r\,\mathrm{d}r,$$

$$I=\sum_{l=1}^{3}\int_{\Omega_l}\zeta_l W',\,\mathrm{Im}\{uv_*\}\,r\,\mathrm{d}r,$$

$$D=\frac{1}{\mathbb{R}}\sum_{l=1}^{3}\int_{\Omega_l}m_l\left[\left(\frac{\mathrm{d}ru}{r\,\mathrm{d}r}\right)^2+\left(\frac{\mathrm{d}rv}{r\,\mathrm{d}r}\right)^2+\left(\frac{\mathrm{d}w}{\mathrm{d}r}\right)^2+\left(\beta^2+\frac{n^2}{r^2}\right)(u^2+v^2+w^2)\right.$$

$$\left.+\frac{4n}{r^2}\mathrm{Re}\{uv_*\}\right]r\,\mathrm{d}r+\frac{1}{\mathbb{R}}[u_{(0)}^2+v_{(0)}^2],\tag{5.3}$$

$$B=\mathrm{Im}\left\{\left[\!\!\left[-pru_*+\frac{\mathrm{i}}{\mathbb{R}}m_l\left(\frac{\mathrm{d}ru}{r\,\mathrm{d}r}ru_*+\frac{\mathrm{d}rv}{r\,\mathrm{d}r}rv_*+\frac{\mathrm{d}w}{\mathrm{d}r}rw_*\right)\right]\!\!\right]_{\eta+b}\right\}.$$

$\dot{E}$ is the rate of change of kinetic energy of the perturbed flow; I is the rate at which energy is transferred from the basic flow to the perturbed flow through the Reynolds stress; $-D$ is the rate of viscous dissipation of the perturbed flow and B is the rate at which energy is being supplied at two interfaces.

Using the interface conditions (3.10)–(3.17), the energy B can be written as

$$B = B_{1\eta} + B_{1b} + B_{2\eta} + B_{2b}, \tag{5.4}$$

where

$$\left.\begin{aligned} B_{1\eta} &= c_i \frac{J^*}{\beta \mathbb{R}^2} \frac{1-n^2-\eta^2\beta^2}{\eta(W(\eta)-c)^2} u^2(\eta), \\ B_{1b} &= c_i \frac{J^*}{\beta \mathbb{R}^2} \frac{1-n^2-b^2\beta^2}{b(W(b)-c)^2} u^2(b), \end{aligned}\right\} \tag{5.5}$$

$$\left.\begin{aligned} B_{2\eta} &= \frac{2(1-m)}{\mathbb{R}}\left[v^2(\eta) - \mathrm{Re}\left\{\eta u'(\eta^+)\, u_*(\eta) + \frac{\eta^2(2-m)}{A(W-c)} u^2(\eta) \right.\right. \\ &\quad \left.\left. + \frac{\eta^2 m}{A\beta(W-c)_*} w'(\eta^+)\, u_*(\eta)\right\}\right], \\ B_{2b} &= -\frac{2(1-m)}{\mathbb{R}}\left[v^2(b) - \mathrm{Re}\left\{b u'(b^+)\, u_*(b) - \frac{b^2(1-2m)}{A(W-c)} u^2(b) \right.\right. \\ &\quad \left.\left. + \frac{b^2}{A\beta(W-c)_*} w'(b^+)\, u_*(b)\right\}\right], \end{aligned}\right\} \tag{5.6}$$

where $(W-c)_*$ indicates the complex conjugate of $(W-c)$.

$B_{1\eta}, B_{1b}$ give the energy supplied at interfaces $r = \eta$ and $r = b$ due to surface tension. Surface tension destabilizes long axisymmetric ($n = 0$) waves $\beta < 1/b$ ($B_{1\eta} > 0$ and $B_{1b} > 0$) and stabilizes short waves $\beta > 1/\eta$ ($B_{1\eta}, B_{1b} < 0$). Surface tension always stabilizes non-axisymmetric perturbations ($n \geqslant 1$). $B_{2\eta}$ and B_{2b} are the energy supplied at interface $r = \eta$ and $r = b$, due to the difference of viscosity of the two fluids.

Since the amplitude of velocities, u, v, w (or eigenfunctions) is arbitrary, the value of each term of energy is normalized with $D = 1$. From the values of $B_{1\eta}, B_{1b}, B_{2\eta}, B_{2b}$, $I, \dot{E}$, we can determine which interface is more unstable, where the instability arises and what kind of instability it is.

6. Comparison with previous results for two-layer core–annular flow

In what follows, we shall give new results for the problem of core–annular flow in two layers. To reduce the three-layer equations to two layers, we suppress all terms relating to the interface $r = b$. In the two-layer case, the basic flow is

$$W(r) = \begin{cases} \{1-\eta^2+m(\eta^2-r^2)\}/A, & r \in [0, \eta], \\ (1-r^2)/A, & r \in [\eta, 1] \end{cases} \tag{6.1}$$

where

$$A = 1-\eta^2(1-m) \tag{6.2}$$

and

$$m_l = (1, m), \quad \zeta_l = (1, \zeta) \quad (l = 1, 2). \tag{6.3}$$

We wish first to specify how many elements are needed to obtain reliable results. Table 1 lists the influence of the number of elements on the eigenvalue c for three

Elements in Ω_1	Elements in Ω_2	c_1	c_2	c_3
3	3	0.38261 + 0.025392i	0.66847 + 0.0039740i	0.67014 + 0.0033849i
5	5	0.38299 + 0.021087i	0.66909 + 0.0041040i	0.67171 + 0.0032618i
10	10	0.38425 + 0.020753i	0.66929 + 0.0041341i	0.67251 + 0.0032652i
15	15	0.38451 + 0.020912i	0.66932 + 0.0041366i	0.67268 + 0.0032688i
20	20	0.38614 + 0.020874i	0.66934 + 0.0041374i	0.67274 + 0.0032702i

TABLE 1. Influence of the number of elements of the eigenvalue

cases: $(J^*, \eta, m, \zeta, n, \beta, \mathbb{R}) = (1000, 0.9, 0.05, 1, 0, 5, 500)$: c_1; $(0, 0.7, 0.5, 1, 0, 10, 37.78)$: c_2; and $(0, 0.7, 0.5, 1, 5, 10, 37.78)$: c_3.

This table shows that even if only ten elements (five in Ω_1 and five in Ω_2) are used, the results are satisfactory; therefore, in most of our calculations, there are only five elements in each flow region (Ω_1 and Ω_2). However, the results were frequently checked by using more elements. We found that for larger Reynolds numbers and small viscosity ratios m, more elements are needed in the region outside the core which is occupied by the less viscous liquid. PJC have already noted that $m \to 0$ is a singular limit.

We compared our calculations with results given by PCJ and Joseph, Renardy & Renardy (1983). The comparison with PCJ is given in figure 1. To understand this comparison, we call attention to the different notations used in this paper and theirs.

$$\left.\begin{aligned} &\text{radius ratio } a = R_2/R_1\text{:} \quad a = 1/\eta, \\ &\text{wavenumber based on } R_1\text{:} \quad \alpha = \beta\eta, \\ &\text{Reynolds number } W_0 R_1/\nu_1\text{:} \quad \mathbb{R}_1 = \mathbb{R}\eta. \end{aligned}\right\} \tag{6.4}$$

Figure 1 shows that numerical results agree very well, and we remark that the agreement shown there is representative, not special. The comparison with the results of Joseph *et al.* (1983) are equally satisfactory.

The pseudo-spectral method of PCJ gives rise to spurious eigenvalues in the discretized system. This problem seems not to arise in the present calculation using finite-element methods. When we do numerical integration of finite-element matrices in (4.1) and (4.2), care must be taken at the first element because $r = 0$ is a singular point. This precaution is especially necessary when $n = 1$ because, in this case, $u(0)$, $v(0)$ need not be zero.

7. The viscous core: $m < 1$

The case $m < 1$, with a viscous core and lubricating annulus was treated by Joseph *et al.* (1983) and PCJ, and we shall give more results for this case. We shall compute eigenfunctions to evaluate different terms in the energy balance in an attempt to identify the mechanisms of instability and the finite-amplitude consequences of these mechanisms by comparing with experiments. All of our computations, both for two-layer flow with $m < 1$ and $m > 1$ and for three-layer flow, show that the axisymmetric mode of perturbation is always the most unstable, although the maximum growth rates for $n = 0$ and $n = 1$ are very close for large $\mathbb{R}$. Therefore, only the results for $n = 0$ are presented in this paper.

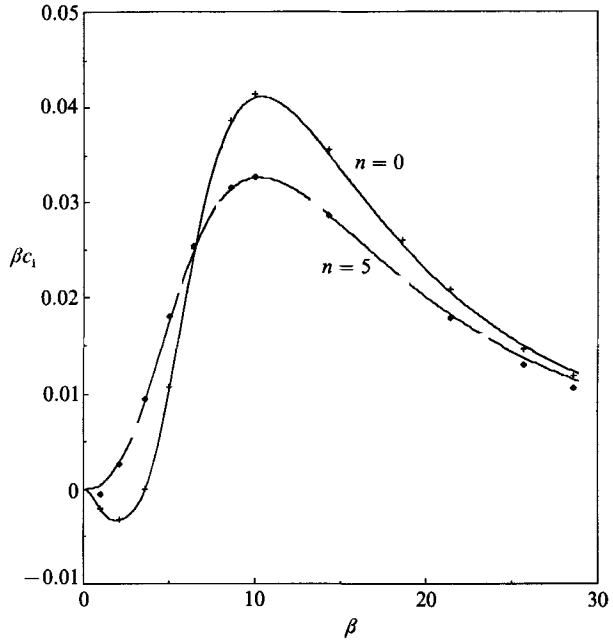

FIGURE 1. Comparison of the present results (solid and dashed lines) with the results of PCJ (+, $n = 0$; ◆, $n = 5$) for $J^* = 0$, $\eta = 0.7$, $m = 0.5$, $\zeta = 1$, $\mathbb{R} = 37.78$. The integer n is the azimuthal mode number.

7.1. *The fastest growing wave*

When J^*, η, m, ζ and $\mathbb{R}$ are fixed the growth rates βc_i vary with wavenumber β; there is a positive maximum growth rate at a certain wavenumber $\tilde{\beta}$ provided the flow is unstable.

Figure 2 shows the variation of the maximum growth rate $\tilde{\sigma} \overset{\text{def}}{=} \tilde{\beta} c_i(\tilde{\beta})$ and corresponding wavenumber β with Reynolds number $\mathbb{R}$ when $J^* = 1000$, $\eta = 0.8$, $m = 0.1$ and $\zeta = 1$. Core–annular flow is stable when $\mathbb{R}_L < \mathbb{R} < \mathbb{R}_U$. In this interval, $\tilde{\sigma} = 0$ at $\tilde{\beta} = 0$. $\tilde{\beta}$ decreases slightly at first, then jumps to zero at $\mathbb{R} = \mathbb{R}_L$, remains zero in the stable region $\mathbb{R}_L < \mathbb{R} < \mathbb{R}_U$, jumps up to certain value at $\mathbb{R} = \mathbb{R}_U$, and finally decreases again. Figure 2 is typical for this case. If the basic core–annular flow has no stable region, the right and left branch of the curve giving the maximum growth rate will merge at certain values of $\mathbb{R}$ but the curve for $\tilde{\beta}$ will have one jump at this $\mathbb{R}$ indicating persistence in switching from one mode of instability to another.

7.2. *Energy analysis for two cases with $m < 1$*

PCJ showed that some neutral curves for $m < 1$ have two branches: a lower branch which is associated with long waves leading to capillary instability caused by surface tension at low $\mathbb{R}$, and an upper branch which is associated with shorter waves at large $\mathbb{R}$. The lower branch ends at wavenumber $\beta = 1/\eta$ in our notation or $\alpha = 1$ in theirs. Neutral curves for $\eta = 0.8$ and $\eta = 0.7$ are shown in figure 3. For $\eta = 0.8$, the neutral curve has two branches; while for $\eta = 0.7$, two branches merge. In the present case, the energy equation (5.2) is defined by (5.3) with $\Omega = \Omega_1 \cup \Omega_2$. The boundary terms B_{1b} and B_{2b} at the second interface are suppressed. For simplicity, we write $B_{1\eta}$ and $B_{2\eta}$ as B_1 and B_2. We computed all the terms in the energy equation $\dot{E} = I - D + B_1 + B_2$ corresponding to the two cases shown in figure 3. The eigen-

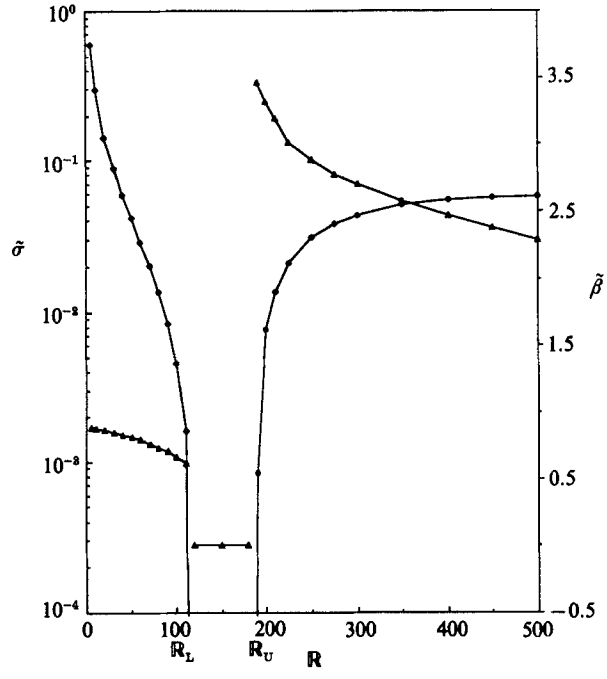

FIGURE 2. The wavenumber $\tilde{\beta}$ of maximum growth and the corresponding growth rate $\tilde{\sigma} = \tilde{\beta} c_i(\tilde{\beta})$ as a function of $\mathbb{R}$: ◆, $\tilde{\sigma}$; △, $\tilde{\beta}$.

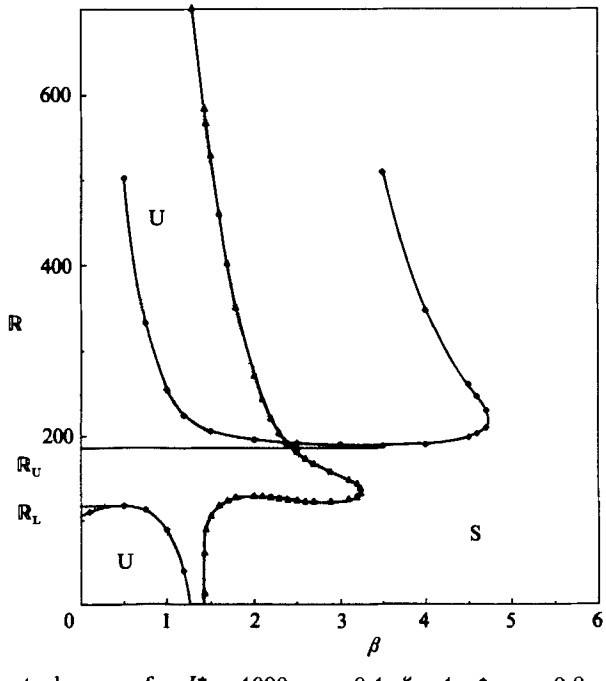

FIGURE 3. Neutral curves for $J^* = 1000$, $m = 0.1$, $\zeta = 1$: ◆, $\eta = 0.8$; △, $\eta = 0.7$. S and U indicate the stable and unstable regions.

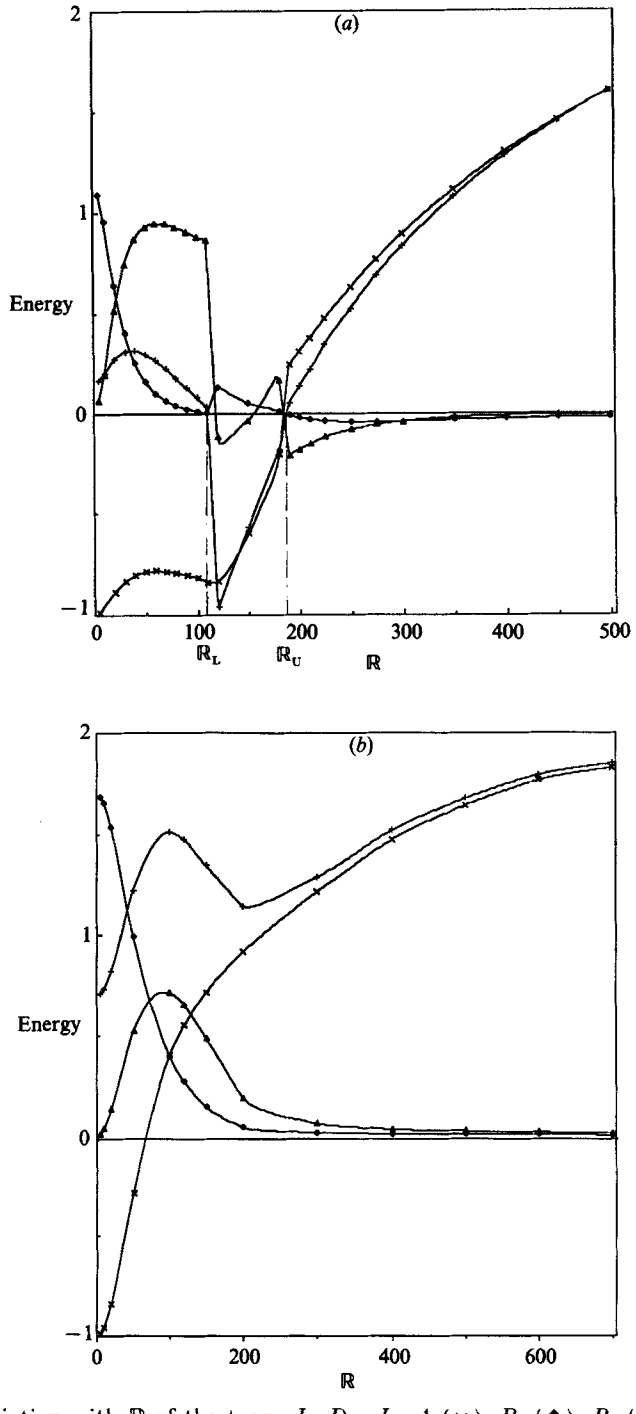

FIGURE 4. Variation with $\mathbb{R}$ of the terms $I-D = I-1$ (×); B_1 (◆); B_2 (△); and E (+) in the energy equation corresponding to the fastest growing disturbance with wavenumber β, $(J^*, m, \zeta) = (1000, 0.1, 1)$. (*a*) $\eta = 0.8$, (*b*) $\eta = 0.7$. Flows with negative $\dot{E}$ are stable. The discontinuities in these curves are caused by mode jumping.

functions in the integrals defining the energy balance are evaluated for $\beta = \tilde{\beta}$, corresponding to the disturbance of fastest growth.

The terms of the energy balance corresponding to $\eta = 0.8$ and $\eta = 0.7$ are plotted as a function of $\mathbb{R}$ in figure 4. Stable core–annular flow with $\mathbb{R}_L < \mathbb{R} < \mathbb{R}_U$ is possible for $\eta = 0.8$, but not for $\eta = 0.7$. Positive values mean that energy is supplied by the disturbance, leading to instability, with the obvious opposite meaning for negative values. There are three different kinds of instability corresponding to:

$B_1 > 0$ (capillary instability due to interfacial tension);

$B_2 > 0$ (surface wave instability due to a difference of viscosity, interfacial friction);

$I-D\,(=I-1) > 0$ (Reynolds stress instability. The production of energy in the bulk of the fluid exceeds its dissipation.)

It is known that B_1, which is proportional to the surface tension parameter J^*, produces capillary instability modified by shear. This instability is always dominant at low $\mathbb{R}$ when $m < 1$. The instability associated with interfacial friction B_2 is destabilizing at the lowest $\mathbb{R}$, but is not as important as capillarity. For larger but still small $\mathbb{R}$ (say, 100), the instability due to interfacial friction dominates interfacial tension. The Reynolds stress minus dissipation terms, $I-1$, of the energy equation, are stabilizing at small $\mathbb{R}$ and destabilizing at large $\mathbb{R}$. Eventually, at large $\mathbb{R}$, the flow is unstable by virtue of the production of energy in the bulk, with negligible contributions from the surface terms B_1 and B_2, as for one fluid. In the stable case $\eta = 0.8$, when there is less water, the Reynolds stress does not grow rapidly and is dominated by the dissipation. When $\mathbb{R}_L < \mathbb{R} < \mathbb{R}_U$, the term $I-D\,(=I-1)$ is stabilizing and overcomes the destabilizing effects of the interfacial friction term B_2. We call this shear stabilization, though what actually happens is that the dissipation is large enough to dominate the other terms when $\mathbb{R}_L < \mathbb{R} < \mathbb{R}_U$. In the case $\eta = 0.8$, $\mathbb{R} > \mathbb{R}_L$ the surface terms are relatively small, but stabilizing.

The energy supplied by the production integral I is associated with the Reynolds stress in Ω and can be decomposed into two parts corresponding to the production of energy in oil Ω_1 and in water Ω_2. In Ω_1, $W' = -2mr/A$ is small when m is small, but $W' = -2r/A$ in Ω_2, which leads to the idea that the instability at higher $\mathbb{R}$ is associated with the water, not the oil. In the two cases corresponding to the conditions specified in figure 4, this idea is verified strongly by computations shown in figure 5 which show that I_1, the Reynolds stress production in the oil, is negligible.

7.3. *Comparison of the energy analysis with experiments*

PCJ determined what types of instability are generated from linear theory and compared their results with experimental results of Charles *et al.* (1961). The density of oil used in the experiments was matched with water by adding carbon tetrachloride. This eliminated gravity effects, so that conditions assumed in the theory (negligible gravity) are achieved in the experiment. In general, the observed flows were far from core–annular flows so that the relevance of results of linearized analysis for actual flows is unknown. Their linearized stability results were in a rather surprising agreement with observed flows with regard to the type of instability and the size of bubbles and slugs, which were computed from the wavelength of the fastest growing disturbances.

We shall now supplement the comparison of theory and experiment by computing all the terms in the energy equation, using the eigenfunctions of the fastest growing mode, for each of the eleven cases shown in figure 6. The computed results are exhibited in table 2. The method used to convert data given for the experiments into

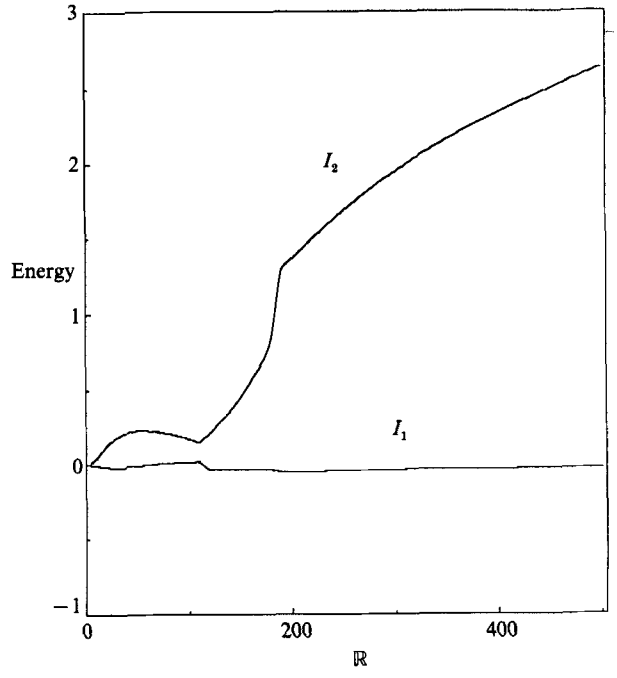

FIGURE 5. The Reynolds stress integral $I = I_1 + I_2$ decomposed into an integral over Ω_1 and Ω_2 with conditions specified in figure 4(*a*).

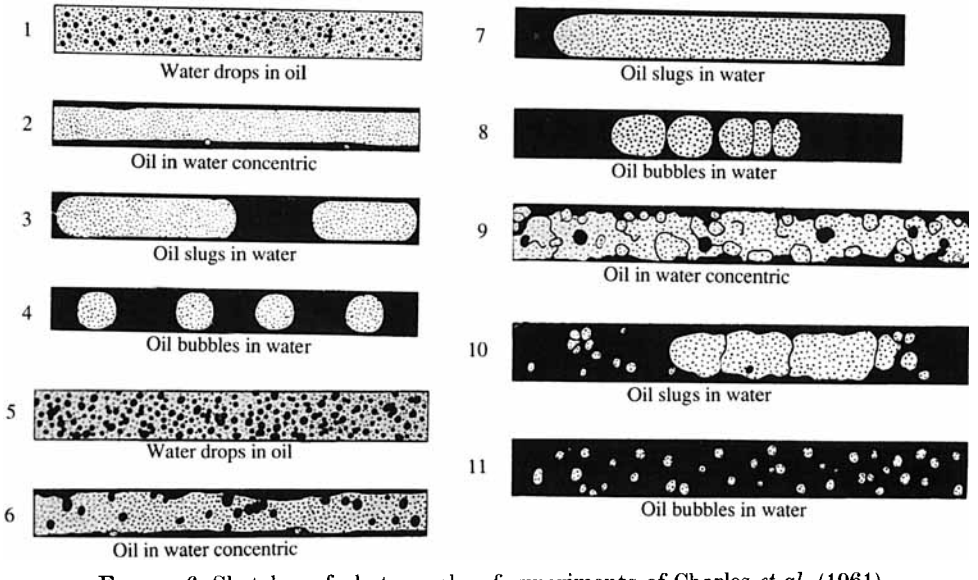

FIGURE 6. Sketches of photographs of experiments of Charles *et al.* (1961).

the values needed for computation is explained by PCJ. Two columns given in the table are not needed for the computations: the volume fraction of water is determined when $\eta = R_1/R_2$ is given, $V_W/V = \pi(R_2^2 - R_1^2)/\pi R_2^2$, and the Reynolds number $\mathbb{R}' = W_0(R_2 - R_1)\rho_2/\mu_2 = \mathbb{R}(1-\eta)\zeta/m$ in the water is determined when the Reynolds number $\mathbb{R}$ and radius ratio are given.

Roughly speaking, two kinds of flow are observed, small water drops in oil and

Exp. No.	η	$\mathbb{R}$	$\mathbb{R}'$	V_W/V	$I-1$	B_1	B_2	$\dot{E}$
1	0.9245	432.2	613.4	0.145	0.361	−0.013	−0.229	0.119
2	0.8260	167.7	548.5	0.318	0.317	−0.008	−0.266	0.043
3	0.7026	99.4	555.40	0.494	0.952	1.408	0.642	3.000
4	0.4460	60.5	630.0	0.801	−0.802	5.784	−0.061	4.921
5	0.7614	833.1	3736.4	0.580	2.521	0.004	−0.015	2.510
6	0.6660	611.1	3836.6	0.556	1.746	0.026	0.034	1.805
7	0.5748	499.9	3995.4	0.670	1.531	0.119	0.241	1.890
8	0.3570	376.8	4554.2	0.873	0.223	4.383	0.275	4.880
9	0.5532	1439.0	12085.4	0.694	0.165	0.001	−0.001	0.165
10	0.3777	1148.2	13430.9	0.857	1.364	0.406	1.011	2.781
11	0.2160	1026.1	15121.5	0.953	−0.276	4.480	0.116	4.319

TABLE 2. Terms of the energy equation $\dot{E} = I-1+B_1+B_2$ evaluated for the most dangerous mode corresponding to the experiments in figure 6

oil bubbles in water. Experiment 2 is an exception: it appears to be a stable core–annular flow but its stability parameters put it close to the border of stability leading to water drops in oil, as in experiment 1. The main factor controlling which phase appears is the water fraction (or radius ratio). There is a phase inversion at a value V_W/V around 0.45 (or η around 0.75) with water emulsions or stable core–annular flow for smaller water fractions and some form of oil bubbles in water for larger water fractions.

According to the linear theory, stable flows are those for which $\dot{E} < 0$. Table 2 shows that the least unstable flow among those in figure 6 is the apparently stable flow of experiment 2. This stable or nearly stable flow is achieved by balancing the destabilizing Reynold stress minus dissipation, $I-1$, against the stabilizing effects of the interface term B_2 associated with the viscosity difference. Capillarity B_1 plays a secondary role.

Emulsions of water drops in oil are seen in experiments 1 and 5. The effects of surface tension B_1 are not important in the linearized theory for these two flows. The instability is produced by the Reynolds stress in the water and is not introduced by effects at the interface which are stabilizing, $B_1+B_2 < 0$. PCJ showed that the emulsifying instability for experiment 1 was for $\mathbb{R} > \mathbb{R}_U$, above the upper critical branch of the neutral curve. The upper and lower critical branches have merged for the larger water fraction in experiment 5. In both experiments, the longest waves are stable.

High Reynolds numbers alone will not emulsify water into oil, as experiment 11 shows. Evidently, water-into-oil emulsions occur at higher Reynolds numbers, above critical, when the water fraction is smaller than a critical value of about 0.45.

At the other extreme, in all the flows where well-defined and fairly uniform size oil bubbles are observed, as in experiments 4, 8 and 11, table 2 shows that the dominating mode instability is due to surface tension, B_1 dominates. The instability of the shorter slugs shown in experiment 3 are still dominated by surface tension.

The interface term B_2, arising from friction, never dominates when $m < 1$. It is an important term in the balance, giving rise to slugs and bubbles in experiments 3, 7, 8 and 10. We shall show in §8 that when $m > 1$, water inside, oil outside, the friction interface term B_2 is the dominant mode of instability giving rise to travelling waves on the interface.

8. The viscous liquid is on the wall: $m > 1$

This case was considered by Hickox (1971) who showed that this flow is always unstable to long waves. He did not consider shorter waves, did not compute maximum growth rates and effectively ignored surface tension. We shall show that this flow is always unstable, surface tension destabilizes long waves at the smallest $\mathbb{R}$ and the friction term B_2 at the interface destabilizes at larger $\mathbb{R}$. The instability takes the form of a travelling wave of growing amplitude. The theory appears to be in good agreement with preliminary results of experiments by W. L. Olbricht and R. W. Aul.

8.1. *Neutral curves, parameters of the fastest growing wave*

Unlike the case $m < 1$, core–annular flow with $m > 1$, the viscous liquid outside, is always unstable. The instability is always greatest for the axisymmetric mode and we shall present results for this case. Typical neutral curves are shown in figure 7. It shows that

$$(\mathbb{R}(\alpha), \alpha) \to (0, 1), \quad \left.\frac{\mathrm{d}\mathbb{R}}{\mathrm{d}\alpha}\right|_{\alpha=1} = \infty.$$

The flow is unstable for small $\mathbb{R}$ when $\alpha < 1$. The results just given appear to be true for all positive values J, m, ζ, so long as $m > 1$.

Figure 8 shows the wavenumber $\tilde{\alpha}$ of the fastest growing wave and the maximum growth rate $\tilde{\sigma}$ as a function of $\mathbb{R}$ for different values η near 1 and $(J, m, \zeta) = (10^5, 10, 1)$. For small $\mathbb{R}$ the wavenumber of the fastest growing wave is independent of η and it is almost constant for $\mathbb{R} < 100$. From figure 8(*b*) it is also evident that $\tilde{\sigma} \to 0$ as $\eta \to 1$. This means that core–annular flow with water in the core and oil outside is only weakly unstable if the thickness of the oil coating is thin.

8.2. *Energy analysis*

In figure 9, we have plotted all the terms in the energy equation $\dot{E} = I - 1 + B_1 + B_2$ when $(J, m, \zeta) = (10^5, 10, 1)$ for $\eta = 0.7$ and 0.99. As in the case $m < 1$, surface tension plays an important role in instability at small values of $\mathbb{R}$, leading to the formation of water drops in oil. The main feature of the flows with $m > 1$ is that the friction term, which is proportional to the viscosity difference, is the dominant mode for instability at all but the smallest $\mathbb{R}$. The instability due to the Reynolds stress is not dominant when $m > 1$. In fact, $I - 1$ is often negative, stabilizing. This property of the Reynolds stress is compatible with the well-known result that Poiseuille flow of one fluid in a round pipe is always stable against all small disturbances governed by the linear theory of stability. When the oil layer is very thin, the flow is only very weakly unstable. This fact, which we noted in our discussion of figure 8, is also evident in figure 9(*b*).

8.3. *Comparison with experiment*

Professor W. L. Olbricht and R. W. Aul of the Department of Chemical Engineering at Cornell University have given us some preliminary results of experiments corresponding to the analysis of this section. Their experimental apparatus is a glass capillary tube of round cross-section of radius 27 μm ($R_2 = 27$ μm). The experiments were arranged so that the glass tube was wetted by UCON oil of the same density as water and water flows in the core. In the results given to us, the film thickness of the oil is 1.8 μm, hence $R_1 = 25.2$ μm. The motion of the fluid is monitored with a microscope. The values of material parameters are: $\rho_1 = \rho_2 = 10^6$ g/m^3, $\mu_1 = 1$ g/ms, $\mu_2 = 173$ g/ms, and $T = 3.5$ g/s^2. Hence $\eta = R_1/R_2 = 0.933$, $m = \mu_2/\mu_1 = 173$, $\zeta = 1$ and $J^* = TR_2\rho/\mu_1^2 = 94.5$.

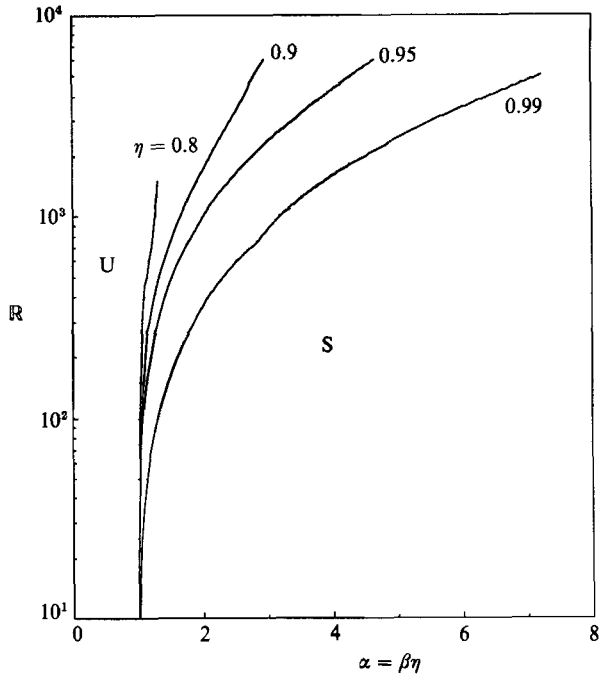

FIGURE 7. Neutral curves for different values of η near 1 when $(J^*, m, \zeta) = (10^5, 10, 1)$. U and S indicate the unstable and stable regions.

The flow data are expressed as a superficial velocity based on the volume flux of water $U = Q_1/\pi R_2^2$. We compute the mass flux of water by integrating the basic velocity (6.1) over the core:

$$Q_1 = W_0 \tfrac{1}{2}\pi R_1^2 \frac{m\eta^2 + 2(1-\eta^2)}{m\eta^2 + (1-\eta^2)}.$$

Thus
$$U = W_0 \tfrac{1}{2}\eta^2 \frac{m\eta^2 + 2(1-\eta^2)}{m\eta^2 + (1-\eta)^2} = 0.436 W_0.$$

We may now form expressions for the following quantities:

centreline velocity: $W_0 = \mathbb{R}\mu_1/\rho_1 R_2 = 3.704 \times 10^4 \mathbb{R}\ \mu\text{m/s}$

superficial water velocity:
$$U = 0.436 W_0 = 1.615 \times 10^4 \mathbb{R}\ \mu\text{m/s}$$

wave length: $L = 2\pi R_2/\tilde{\beta} = 169.6/\tilde{\beta}\ \mu\text{m}$

growth rate: $\tilde{\Sigma} = \tilde{\sigma} W_0/R_2 = 1.372 \times 10^3 \tilde{\sigma}\mathbb{R}\ \text{s}^{-1}$

wave speed $\tilde{C} = c_r(\tilde{\beta})\, W_0 = c_r(\tilde{\beta})\, 3.704 \times 10^4 \mathbb{R}\ \mu\text{m/s}$

where $\tilde{\sigma} = \tilde{\beta} c_i(\tilde{\beta})$.

The superficial water velocities U, which were specified in the experiments, range from 299 μm/s to 697 μm/s, corresponding to $0.0185 < \mathbb{R} < 0.0432$, with an average $U = 448$ μm/s and an average $\mathbb{R} = 0.0277$. The wavelengths observed in the experiments ranged between 200 μm $< L <$ 280 μm, with an average $L = 225$ μm. At the time of writing, measurements of the wave speed had not been carried out.

The prediction of theory for the conditions specified in the experiments are given

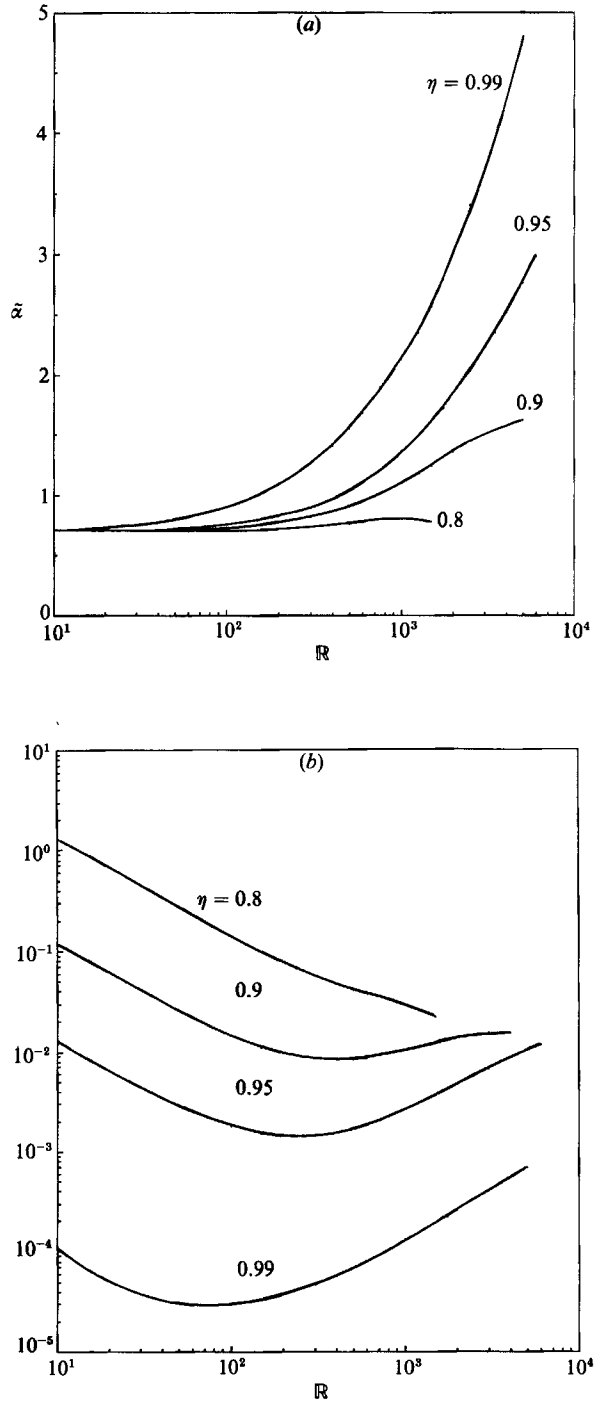

FIGURE 8. Maximum growth rate $\tilde{\sigma}$ and corresponding wavenumber $\tilde{\alpha} = \tilde{\beta}\eta$ against $\mathbb{R}$ for different values of η near 1 when $(J^*, m, \zeta) = (10^5, 10, 1)$. (*a*) $\tilde{\alpha}$, (*b*) $\tilde{\sigma}$.

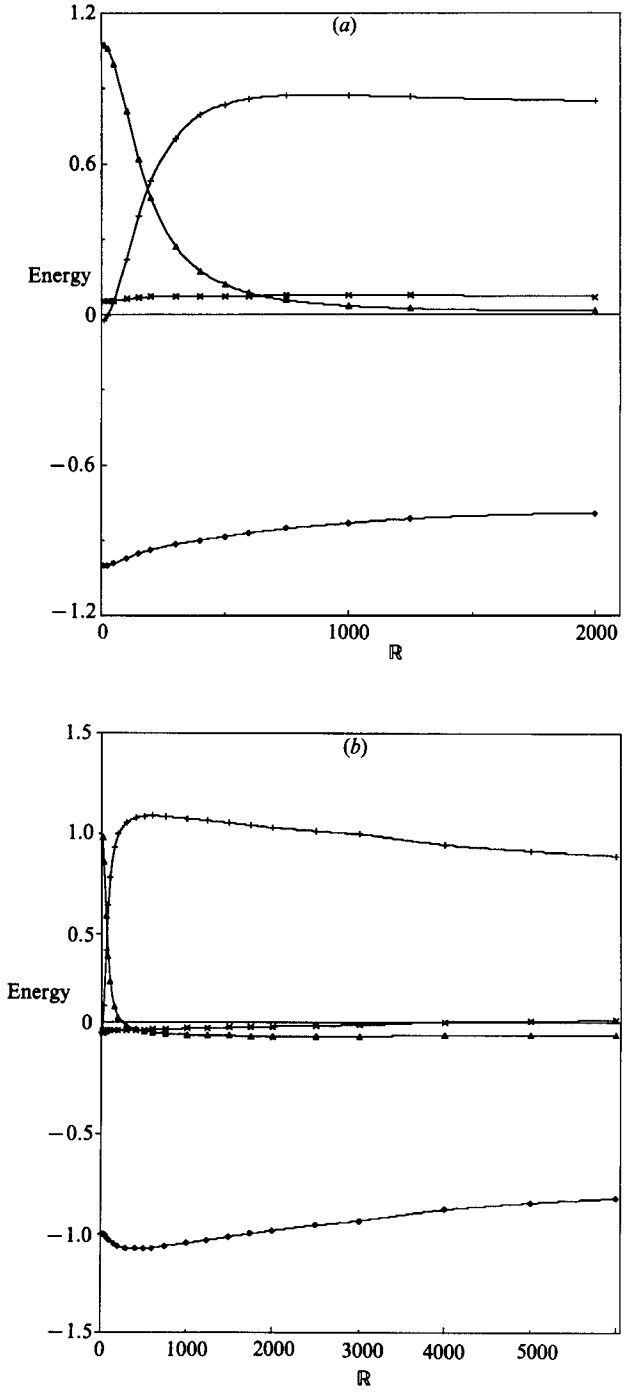

FIGURE 9. Variation of the terms of the energy equation $\dot{E} = I-1+B_1+B_2$ with $\mathbb{R}$ for $(J^*, m, \zeta) = (10^5, 10, 1)$. ◆, $I-1$; △, B_1; +, B_2; ×, $\dot{E}$. (*a*) $\eta = 0.7$, (*b*) $\eta = 0.99$. The flow is unstable for all $\mathbb{R}$, $\dot{E} > 0$. When $\eta = 0.99$, though $\dot{E} > 0$ it is very nearly equal to zero, evidently with neutral stability as $\eta \to 1$.

$\mathbb{R}$	$\tilde{\beta}$	$\tilde{\sigma}$	c_r	L (μm)	$\tilde{\Sigma}(1/s)$	$\tilde{C}$ (μm/s)
0.005	0.757	3.594×10^{-3}	9.900×10^{-4}	224.0	2.465×10^{-2}	0.1833
0.01	0.757	1.797×10^{-3}	9.900×10^{-4}	224.0	2.465×10^{-2}	0.3667
0.0277	0.757	6.488×10^{-4}	9.900×10^{-4}	224.0	2.466×10^{-2}	1.016
0.05	0.757	3.595×10^{-4}	9.900×10^{-4}	224.0	2.466×10^{-2}	1.833
0.1	0.757	1.799×10^{-4}	9.900×10^{-4}	224.0	2.468×10^{-2}	3.667

TABLE 3. Predicted values of the lengths of the fastest growing wave L, the growth rate $\tilde{\Sigma}$ and the wave speed $\tilde{C}$ for the conditions in the experiments of R. W. Aul and W. L. Ulbricht

$\mathbb{R}$	$I-1$	B_1	B_2	$\dot{E}$
0.005	$0.21\times10^{-6}-1$	0.6605	0.3393	0.2117×10^{-6}
0.01	$0.41\times10^{-6}-1$	0.3264	0.6733	0.4173×10^{-6}
0.0277	$0.55\times10^{-6}-1$	0.05934	0.9402	0.5816×10^{-6}
0.05	$0.49\times10^{-6}-1$	0.01899	0.9805	0.6065×10^{-6}
0.1	$0.16\times10^{-6}-1$	0.4819×10^{-2}	0.9946	0.6155×10^{-6}

TABLE 4. Values of the Reynolds stress minus dissipation $I-1$, the interfacial tension surface term B_1, the frictional term at the interface due to the viscosity difference B_2 and the rate of change of disturbance energy $\dot{E}$ for the conditions in table 3

in table 3. We find that the critical wavelength L does not depend on $\mathbb{R}$ for small $\mathbb{R}$. In table 4, we computed terms of the energy balance. The flows are always unstable with small growth rates. The Reynolds stress minus dissipation, $I-1$, is always negative, stabilizing. At the smallest $\mathbb{R}$, the instability is due to a combination of capillarity and interfacial friction. At larger $\mathbb{R}$, in the region of the experiments, capillarity (B_1) has been suppressed and interfacial friction (B_2) supplies the destabilizing mechanism.

The following are points of comparison between theory and experiment:

(1) The theory predicts instability in all situations and no stable flows are observed.

(2) The theory predicts instability to axisymmetric disturbances and only these are observed.

(3) The theory predicts a travelling wave whose amplitude is increasing. This type of wave is always observed.

(4) The theory predicts that the wavenumber of the fastest growing wave is independent of $\mathbb{R}$ in the range of small $\mathbb{R}$ in the experiments. This also appears to be true of the experiments though there is a non-systematic variation in the observed values of L, $200 < L < 280$, which does not correlate with $\mathbb{R}$.

(5) The value of $L = 224$ is predicted and a mean value $L = 225$ is observed.

9. Stability of thin liquid threads

When η is sufficiently small, the core degenerates into a thin thread with a velocity profile

$$W(r) \sim \begin{cases} 1, & r\in[0,\eta], \\ 1-r^2, & r\in[\eta,1] \end{cases}$$

independent of m when $m\eta^2 \ll 1$. Moreover, both $W'(\eta^-)$ and $W'(\eta^+)\to 0$ with η. We may, therefore, expect limiting results, giving the instability of a uniform jet at the

centre of a Poiseuille flow of another liquid. The Poiseuille flow of a single liquid in a round pipe is always stable to small disturbances, and this stability does not appear to be disturbed by the small diameter, unstable jet. The jet itself cannot depend on W in this limit of small η and, if a new eigenvalue $\tilde{c} = \mathbb{R}(1-c)$ is defined, then it can be easily verified that the interface conditions are independent of $\mathbb{R}$. In fact, our numerical results do give the eigenvalue c proportional to $1/\mathbb{R}$ and limiting values of the neutral curve and wavenumbers of the fastest growing wave which are independent of $\mathbb{R}$. PCJ examined a capillary jet limit for a very viscous core, and it reduced to one treated by Chandrasekhar (1961) in which $J(=TR_1\rho_1/\mu_1)$, rather than $\mathbb{R}$, appears as the controlling parameter. The thin jets studied here also have this property. The analysis of the energy of these jets shows clearly that when $\eta \to 0$, we are dealing exclusively with capillary instability. The disturbance energy associated with the Reynolds stress minus dissipation and with interfacial friction is stabilizing.

9.1. *Neutral curves, parameters of the fastest growing wave*

The parameters used in this section are the wavenumber $\alpha = \eta\beta$ which is made dimensionless with R_1, the usual Reynolds number $\mathbb{R} = \rho_1 R_2 W_0/\mu_1$ and the surface-tension parameter $J^* = TR_2\rho_1/\mu_1^2$. We shall give results for two representative values, $m = 0.1$ and $m = 10$, and confine our attention to the case of matched density $\rho_2 = \rho_1$. If $\mathbb{R}$ and J^* are for $m = 0.1$, then $10\mathbb{R}$ and $100J^*$ are the Reynolds number and surface-tension parameter when $m = 10$. We are comparing two fluids with the same density and different viscosities when the thin jet with $\eta = R_1/R_2$ is less or more viscous, say, oil inside and water outside or vice versa.

Figure 10 shows that the neutral curves are independent of $\mathbb{R}$ for small $\mathbb{R}$ and are also independent of m for small $\mathbb{R}$. The neutral curves begin at $\mathbb{R} = 0$ and $\alpha = 1$, and it appears that $\partial\mathbb{R}/\partial\alpha = \infty$. The flow is unstable for wavenumbers on the left of the neutral curves. Neutral curves of this sort are characteristic for capillary instability in which the main action of viscosity enters through J^* rather $\mathbb{R}$.

Figure 11 shows the maximum growth $\tilde{\sigma}^* = \tilde{\alpha}c_i(\tilde{\alpha})$, as a function of $\mathbb{R}$ for different η. The straight lines are proportional to $1/\mathbb{R}$, consistent with the interpretation that $\tilde{c} = \mathbb{R}(1-c)$ is the relevant eigenvalue, rather than c. We also noted that the wavenumber of the fastest growing wave is basically independent of $\mathbb{R}$ for small η, irrespective of whether the more viscous liquid is inside or outside.

Table 5 shows that the instability of the thin jet is due to capillarity. There are only weak effects of $\mathbb{R}$ and m through the stabilizing action of the Reynolds stress minus dissipation, $I-1$, and the interfacial friction B_2.

9.2. *Capillary instability*

In the study of instability of jets, it is appropriate to use the radius of the jet R_1 as the scale of length. We have introduced dimensionless parameters $J = TR_1\rho_1/\mu_1^2$ and $\mathbb{R}_1 = W_0 R_1\rho_1/\mu_1$, and the wavenumber α based on R_1.

Consider the capillary instability of a liquid jet in air. This corresponds to core-annular flow with a liquid core and an air annulus. Therefore, we take the viscosity ratio m and density ratio ζ to be very small. If the influence of the air is neglected and the jet is considered inviscid, this capillary instability leads to Rayleigh's result that the maximum growth rate occurs for the wavenumber $\tilde{\alpha} = 0.697$. The jet presumably breaks into bubbles of length $2\pi R_1/0.697$ because of surface tension. Table 6 lists the results of present computations, where J is taken very large and $\mathbb{R}_1$ very small to ensure that surface tension dominates the instability. The agreement with Rayleigh's $\tilde{\alpha} = 0.697$ is excellent.

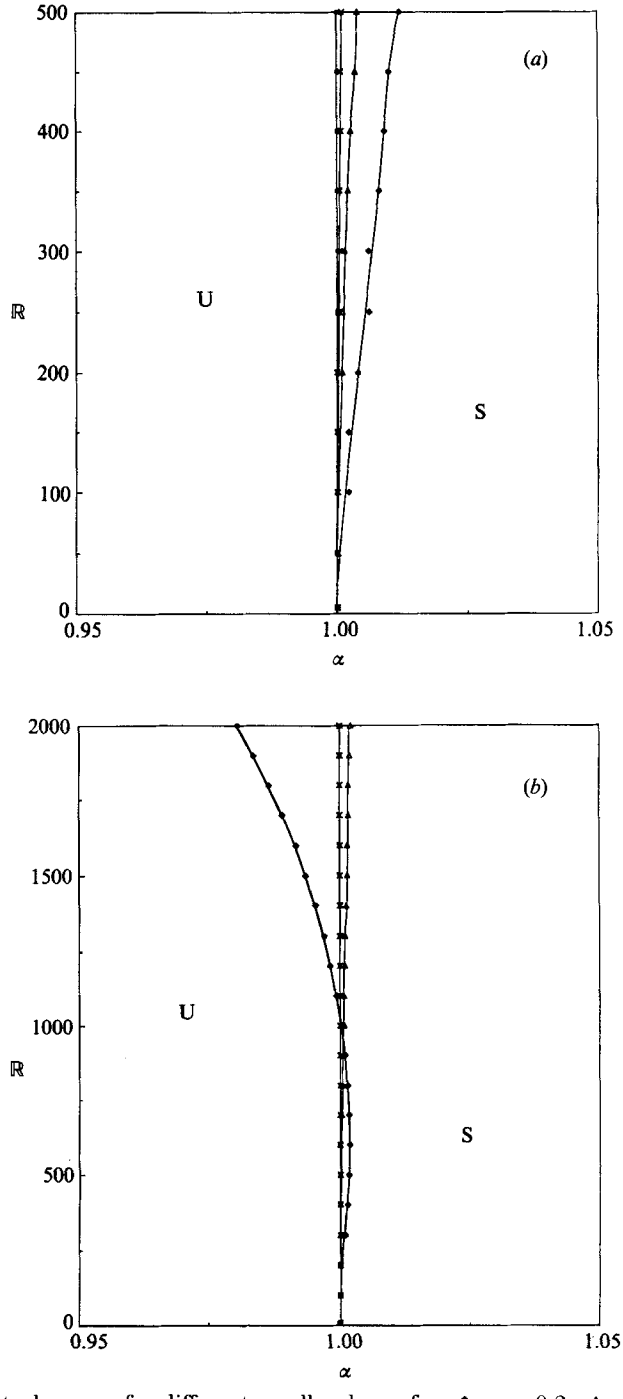

FIGURE 10. Neutral curves for different small values of η. ◆, $\eta = 0.2$; △, $\eta = 0.1$; ×, $\eta = 0.05$; ■, $\eta = 0.01$. (*a*) $(J^*, m, \zeta) = (10^3, 0.1, 1)$; (*b*) $(J^*, m, \zeta) = (10^5, 10, 1)$.

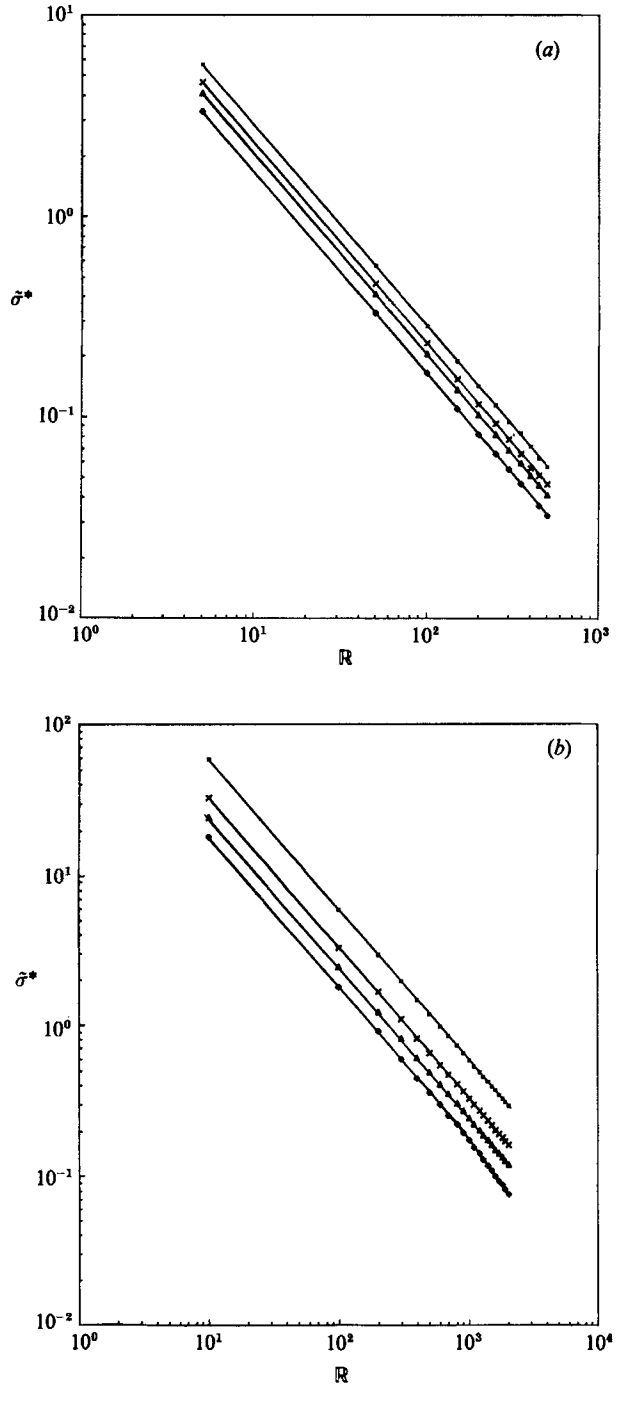

FIGURE 11. Maximum growth rate $\tilde{\sigma}^*$ as a function of $\mathbb{R}$ for $\eta = 0.2$, 0.1, 0.05 and 0.01. Symbols as in figure 10.

$\mathbb{R}$	B_1	B_2	$I-1$	$\dot{E}$
	$(J^*, m, \eta, \zeta) = (1000, 0.1, 0.05, 1)$			
5	2.422	−0.05065	$0.1141\times10^{-5}-1$	1.3717
50	2.422	−0.05063	$0.1140\times10^{-3}-1$	1.3716
100	2.422	−0.05059	$0.4545\times10^{-3}-1$	1.3723
250	2.422	−0.05026	$0.2793\times10^{-2}-1$	1.3748
500	2.421	−0.04919	$0.1058\times10^{-1}-1$	1.3829
	$(J^*, m, \eta, \zeta) = (10^5, 10, 0.05, 1)$			
10	3.681	−0.2285	$0.4840\times10^{-7}-1$	2.4523
100	3.681	−0.2285	$0.4840\times10^{-5}-1$	2.4523
500	3.680	−0.2283	$0.1210\times10^{-3}-1$	2.4522
2000	3.672	−0.2250	$0.1914\times10^{-2}-1$	2.4490

TABLE 5. Terms of the energy balance for thin liquid threads

η	0.8	0.6	0.4	0.2	0.1	0.05
$\tilde{\alpha}$	0.6970	0.6969	0.6968	0.6968	0.6967	0.6965

TABLE 6. Capillary instability of a liquid jet in air $(J, m, \zeta, \mathbb{R}_1) = (10^{10}, 10^{-3}, 10^{-4}, 10^{-3})$

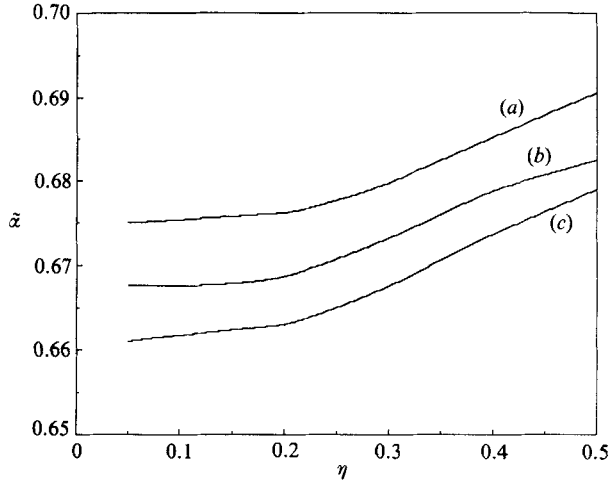

FIGURE 12. The wavenumber $\tilde{\alpha}$ of the fastest growing wave as a function of η when the density is matched, $\zeta = 1$, and capillary instability dominates. (a) $(J, \mathbb{R}_1, m) = (10^{10}, 0.1.0.1)$; (b) $(J, \mathbb{R}_1, m) = (2\times10^9, 10^{-3}, 10^3)$; (c) $(J, \mathbb{R}_1, m) = (2\times10^3, 10^{-3}, 10^{-3})$.

In the above case, the inertia of fluid outside the jet could be neglected. Now let us consider another extreme case, a jet of air injected into liquid. The capillary instability of such a 'hollow jet' was studied by Chandrasekhar (1961) with the result that the maximum growth rate is achieved at $\tilde{\alpha} = 0.484$. It is obvious that in this situation the boundary of the pipe wall will have an effect on the instability, but this effect should become less as the core becomes thinner. In our computation, m and ζ are both taken very large to simulate the situation, and we find that at $\eta = 0.1$, $\tilde{\alpha} = 0.489$ and at $\eta = 0.05, \tilde{\alpha} = 0.487$, which is very close to Chandrasekhar's result of 0.484.

For $\zeta = 1$, the inertia of both the fluid in the core and in the annulus cannot be neglected. Figure 12 presents results for three cases. For all the cases, the calculated limit $\tilde{\alpha}$ as $\eta \to 0$ depends on the value of J and m. Computations show that for very large J, where surface tension plays a dominant role, the limiting value $\tilde{\alpha}$ is almost the same for different viscosity ratios m regardless of whether $m < 1$ or $m > 1$. For certain m, the limiting value increases with J and also tends to a unique J-independent limiting value when J is large.

10. Stability of core–annular flow in three layers (hydrophobic pipe walls)

For certain construction materials, it is impossible to make the water wet the pipe wall; the pipe wall is hydrophobic and takes on oil preferentially. Teflon is an example. It is possible to get a lubricated flow in such a situation. There is an annulus of water between the oil in the core and the oil on the wall. In fact, we shall show that core–annular flow of this type is always unstable. In these cases, we see waves on the surface of the oil that wet the wall. It appears that such waves are equilibrated nonlinearly and that they are driven by an instability due to friction at the interface. In this section, we give the results from the linear theory of stability for the three-layer problem. The finite-element code used in this paper works well for the three-layer problem. Here, we give a sample of results restricted to the case of density-matched fluids $\zeta = 1$ and based on a comparison with two representative two-layer problems. The representative problems are for $\eta = 0.6$ and $\eta = 0.8$. when $\eta = 0.8$, the neutral curve has two branches; whereas for $\eta = 0.6$ the neutral curve is continuous and not in separate branches.

10.1. *Neutral curves*

In figure 13 we present neutral curves for the three-layer problem. To the left of the neutral curve is the unstable region and to the right is the stable region. The flow is always unstable to long waves, as in the two-layer case with $m > 1$. The neutral curves all begin at a wavenumber $\beta = 1/\eta$. The neutral curves for $b = 0.90$ and $b = 0.95$ in figure 13(*a*) have a corner at a certain β-value; the neutral curves for $b = 0.8$ and $b = 0.9$ in figure 13(*b*) are rather strange. These unusual features will be explained in what follows.

Actually, three-layer core–annular flow can be regarded as composed of one two-layer flow with $m < 1$ and another two-layer flow with $m > 1$, as shown in figure 14. Decomposing the flow into these two parts, we define the dimensionless parameters $\mathbb{R}, J^*$ based on one fluid (fluid 1), as in (3.2), for all three cases. This decomposition will provide the explanation of the main features of the neutral curves. In figure 15, we compare two- and three-fluid neutral curves when $\eta = 0.8$ and 0.6. The neutral curve for the three-layer case (1) begins at $\beta = 1/\eta$, first following the lower branch of the neutral curve for case (2), then following the neutral curve for case (3) until it meets the upper branch of the neutral curve for case (2). At this point, it makes a sharp turn to the right, roughly following the upper branch. Since the upper branch of the neutral curve corresponds to instability due to Reynolds stress in the water layer, the real characteristic length for this instability is the thickness of the water layer. When another layer of fluid is added near pipe wall, this characteristic length decreases, correspondingly the wavenumber β increases; therefore, the position of this part of neutral curve for three-layer case moves to larger β, as seen in figure 15(*a*). The increase of wavenumber for this part of the neutral curve is not linearly proportional to the decrease of the thickness of the layer; computation shows that Reynolds stress near the pipe wall gives a relatively larger contribution to the total

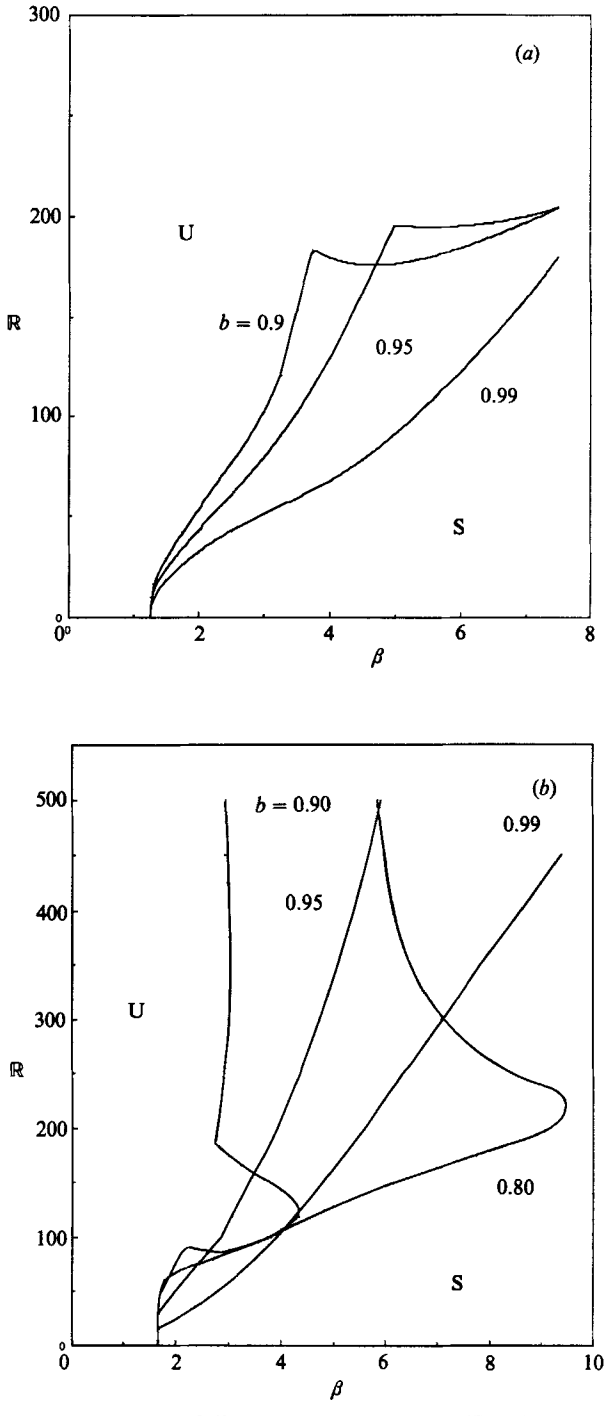

FIGURE 13. Neutral curves for different values of $b = R_2/R_3$ when $J^* = 10^3$, $m = 0.1$ and (a) $\eta = 0.8$, (b) $\eta = 0.6$.

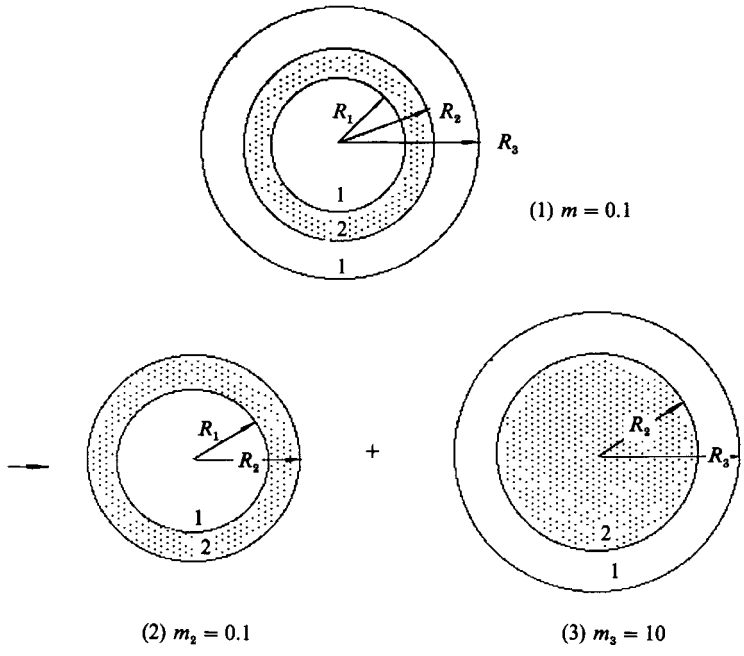

FIGURE 14. Diagram showing how three-layer core–annular flow could be understood from the composition of two two-layer flows.

integrated Reynolds stress in the water. This is also seen in figure 15(*b*) where the neutral curve for case (3) has a sharp cut on the deformed horseshoe-shaped neutral curve (2). It is expected that as the outer layer becomes thinner ($b \to 1$), this deviation of the neutral curve becomes less. Therefore, the neutral curve for the three-layer flow can be viewed as a combination of neutral curves for case (3) and the deformed neutral curve for case (2) in which upper branch is moved to larger β.

10.2. *Parameters of the fastest growing wave*

In the three-layer problem, $b = R_2/R_3$, $\eta \leqslant b \leqslant 1$, is the radius of the interface nearest the wall at $r = 1$ and $\eta = R_1/R_3$ is the radius of the core. The case in which a thin oil layer is on the wall, $b \to 1$, is of practical interest. In figure 16, we have plotted the growth rate $\sigma(\beta)$ for $(J^*, m, \eta) = (10^3, 0.1, 0.8)$ for different $\mathbb{R}$ and (*a*) $b = 0.9$, (*b*) $b = 0.99$. Discontinuities in the slopes of the curve mean that the mode of instability has changed. For example, the growth rate curve for $\mathbb{R} = 200$, shown in figure 16(*a*), has two peaks: energy analysis shows that the first peak is associated with interfacial friction, the second with an instability due to the Reynolds stress in the middle (water) layer. As $\mathbb{R}$ increases, the second peak grows and becomes dominant at $\mathbb{R} = 500$. The magnitude of the growth rates decreases as $b \to 1$. In figure 16(*b*), we have plotted the growth rates on a logarithmic scale. The first peak on the curve for $\mathbb{R} = 50$ is due to instability induced by interfacial tension and friction on the interface at $r = \eta$. The high peak on the curve for $\mathbb{R} = 500$ corresponds to an instability due to the Reynolds stress in the water layer. The curve for $\mathbb{R} = 150$ is smooth because there is only one unstable mode due to interfacial friction; the corresponding two-layer flow is stable when $\mathbb{R} = 150$ (see figure 3).

Figure 17 shows the maximum growth rate $\tilde{\sigma} = \tilde{\beta} c_i(\tilde{\beta})$ and wavenumber $\tilde{\beta}$ of the fastest growing wave as a function of $\mathbb{R}$ for the conditions specified in figure 16 when

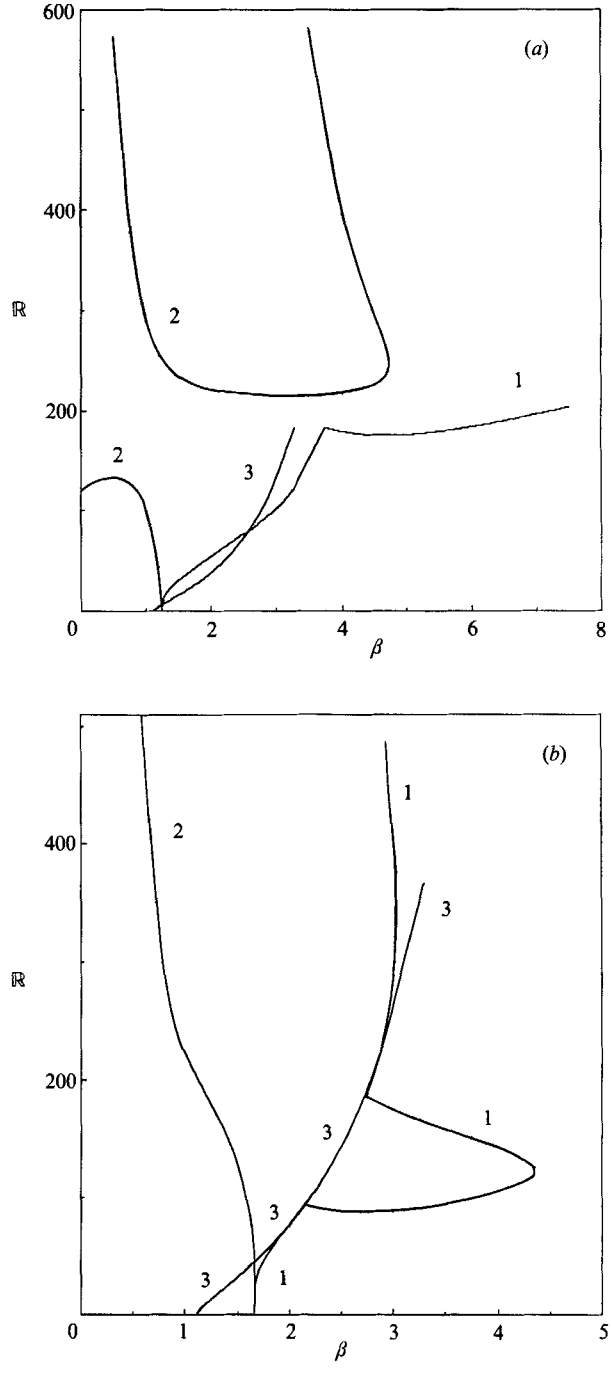

FIGURE 15. Neutral curves for two-layer and three-layer flows when $(J^*, m, b) = (10^3, 0.1, 0.9)$. (1) Three layers; (2) two layers with $m = 0.1$; (3) two layers with $m = 10$. (*a*) $\eta = 0.8$, (*b*) $\eta = 0.6$.

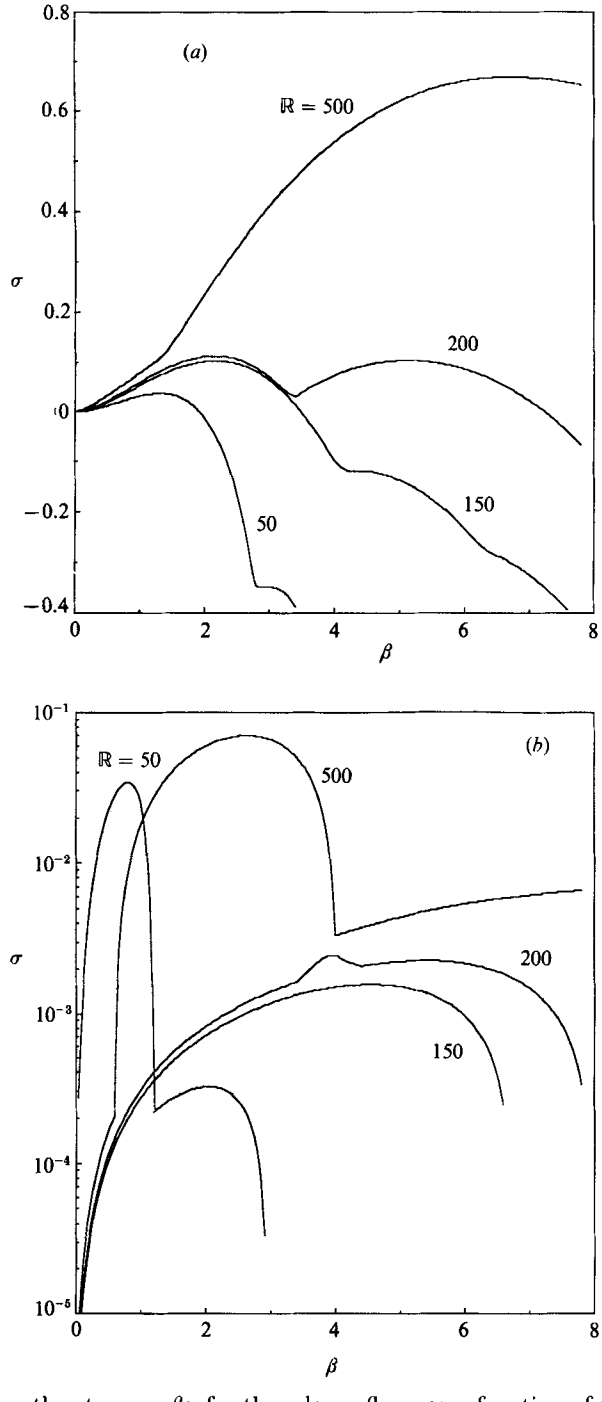

FIGURE 16. Growth rates $\sigma = \beta c_i$ for three-layer flows as a function of the wavenumber and different $\mathbb{R}$ when $(J^*, m, \eta) = (10^3, 0.8, 0.1)$. (*a*) $b = 0.9$, (*b*) $b = 0.99$.

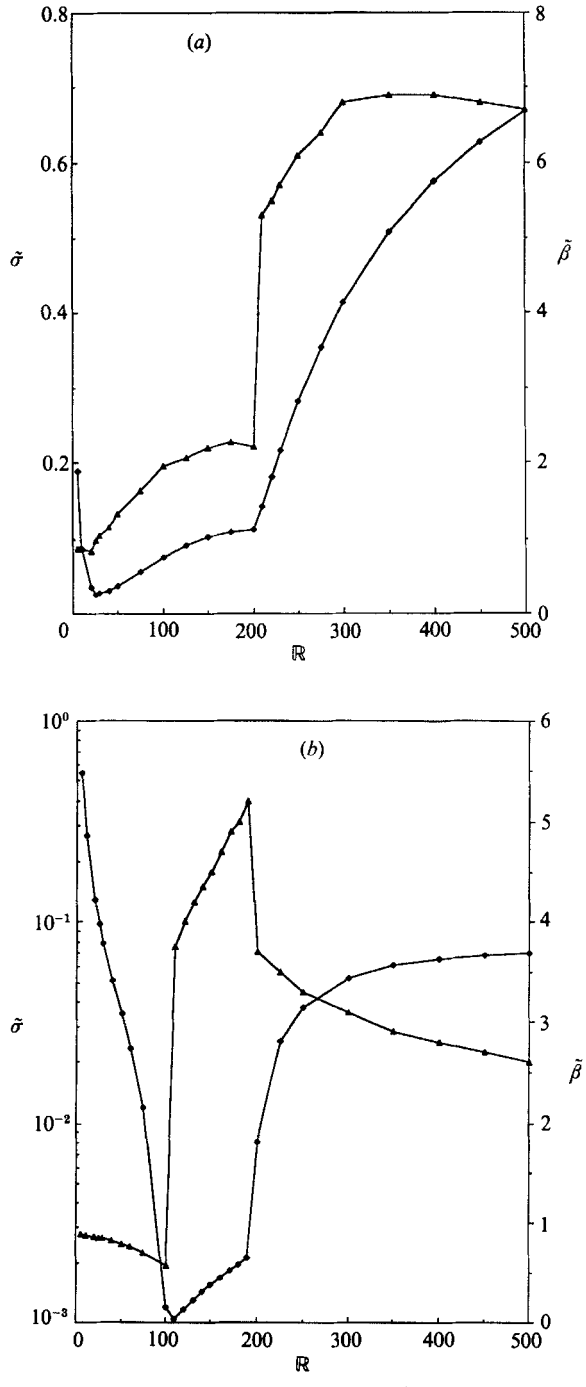

FIGURE 17. Maximum growth rates $\tilde{\sigma}$ and wavenumber $\tilde{\beta}$ for maximum growth as a function of $\mathbb{R}$ when $(J^*, m, \eta) = (10^3, 0.8, 0.1)$. ◆, $\tilde{\sigma}$; △, $\tilde{\beta}$. (*a*) $b = 0.90$, (*b*) $b = 0.99$.

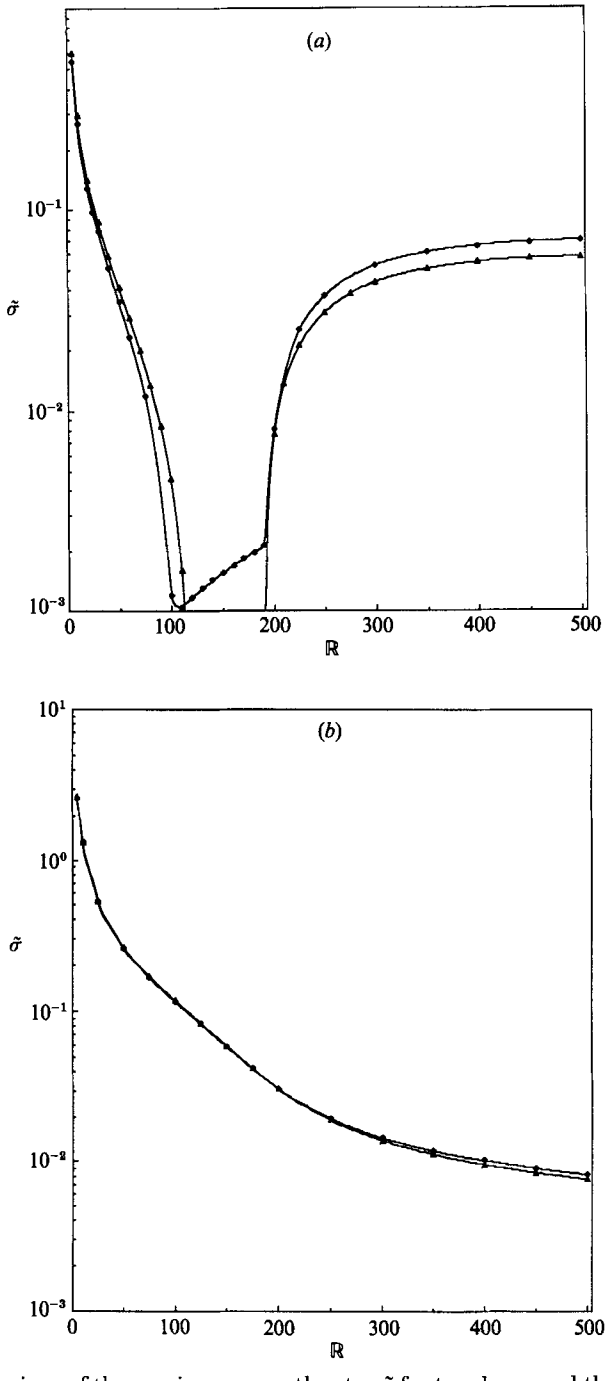

FIGURE 18. Comparison of the maximum growth rates $\tilde{\sigma}$ for two-layer and three-layer core–annular flow when the viscous layer on the outer wall is thin, $(J^*, m, b) = (10^3, 0.1, 0.99)$. ◆, Two layers; △, three layers. (*a*) $\eta = 0.8$, (*b*) $\eta = 0.6$.

$\eta = 0.8$. The corresponding two-layer flow for $\eta = 0.8$ has an interval, shown in figure 3, in which core–annular flow is stable. The curves in figure 17 can be divided into three regions. The first is a region of small $\mathbb{R}$ where the growth rate for interfacial tension and friction is larger at the inner than at the outer interface. The second region is for medium $\mathbb{R}$ where the growth rate for instability at the outer interface dominates; actually the inner interface is stable for most values of $\mathbb{R}$ in this section. Since the growth rate for the outer interface tends to zero as $b \to 1$, when $b = 0.99$ (figure 17*b*), the boundary of this region is quite sharp and just fits the stable region of two-layer flow in figure 3. The third region is for larger $\mathbb{R}$ where the growth rate for the inner interface again is the larger one and the flow is unstable due to the growth of the Reynolds stress. The jumps of $\tilde{\beta}$ indicate changes in the dominant mode of instability. The case $\eta = 0.6$ usually does not exhibit mode jumping, because the corresponding neutral curve for the two-layer problem shown in figure 3 does not have distinct branches. In all the cases, the growth rate for instability is larger at the inner than at the outer interface.

Figure 18 demonstrates that the difference between the two- and three-layer cases tends to zero as the outer layer gets thinner, $b \to 1$. A thin layer of oil on the wall of a pipe need not be a serious impediment to the lubrication of an oil core with water.

10.3. *Energy analysis*

In three-layer core–annular flow, there are two interfaces and three flow regions; the instabilities are more complicated than in two-layer flow. But using energy analysis, we can again determine the source of these instabilities.

Figure 19 shows the graph of the terms in the energy equation, $\dot{E} = I - D + B_{1\eta} + B_{1b} + B_{2\eta} + B_{2b}$, corresponding to the growth rate curves shown in figure 17. These curves are associated with mode jumping which is evident from figure 17. In the first region, $B_{1\eta}$ and $B_{2\eta}$ are destabilizing. The instability is induced at the inner interface. As $\mathbb{R}$ increases, the first instability is a capillary instability due to interfacial tension ($B_{1\eta}$); then interfacial friction $B_{2\eta}$ becomes important. At higher $\mathbb{R}$, in the second region, B_{2b} is largest; the instability is due to the interfacial friction at the outer interface (we believe this produces waves at the outer interface). At still higher $\mathbb{R}$, in the third region, instability due to the Reynolds stress becomes dominant. This type of instability can be associated with the formation of emulsions of water in oil, at least in some cases.

In lubricated pipelining, core–annular flow with capillary instability (oil bubbles or oil slugs in water) or surface waves is also effective for lubricated transport of very viscous oil, although not as effective as stable core–annular flow. The most undesirable situation is when water emulsifies in the oil. This leads to breakdown of lubrication. The results of linearized stability theory suggest that the oil layer at the pipe wall does not have much influence on the operation of lubricated pipelining since it induces only slight changes in the onset of instabilities due to the Reynolds stress in the water.

Hooper & Boyd (1987) studied the instability of Couette flow of two superposed fluids of different viscosity when the depth of the lower less viscous fluid is bounded by a wall and the interface, while the depth of the upper viscous fluid is unbounded. They studied a finite-amplitude instability revealed first in a numerical study of Y. Renardy (1985) and suggested that the instability is due to the disturbance vorticity generated by the solid boundary. They showed that this instability is driven by the Reynolds stress in the water when $m < 1$. In fact, the Reynolds stress is proportional to W', where $W(r)$ is the forward velocity of the basic flow. W' in the water is about

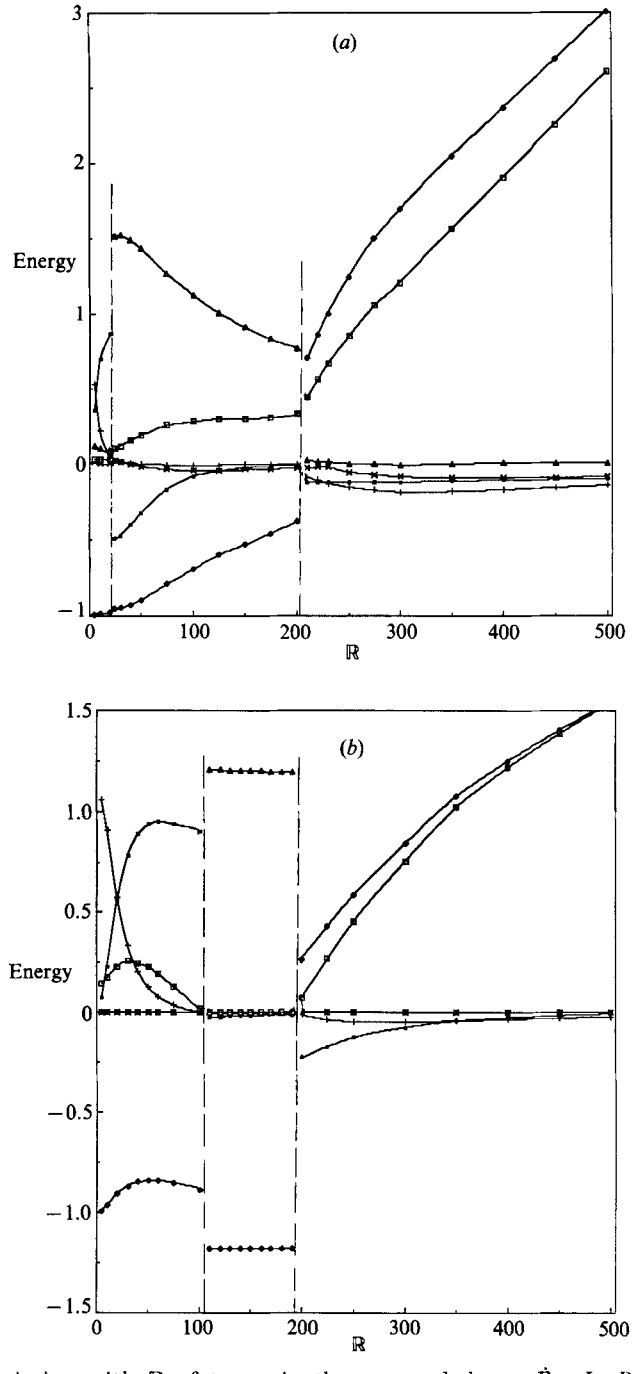

FIGURE 19. Variation with $\mathbb{R}$ of terms in the energy balance $\dot{E} = I + B_{1\eta} + B_{2\eta} + B_{1b} + B_{2b} - D$, normalized for $D = 1$ with $(J^*, m, \eta) = (10^3, 0.1, 0.8)$. (*a*) $b = 0.9$, (*b*) $b = 0.99$. ◆, $I-1$; +, $B_{1\eta}$; ×, B_{1b}; ■, $B_{2\eta}$; △, B_{2b}; □, $\dot{E}$.

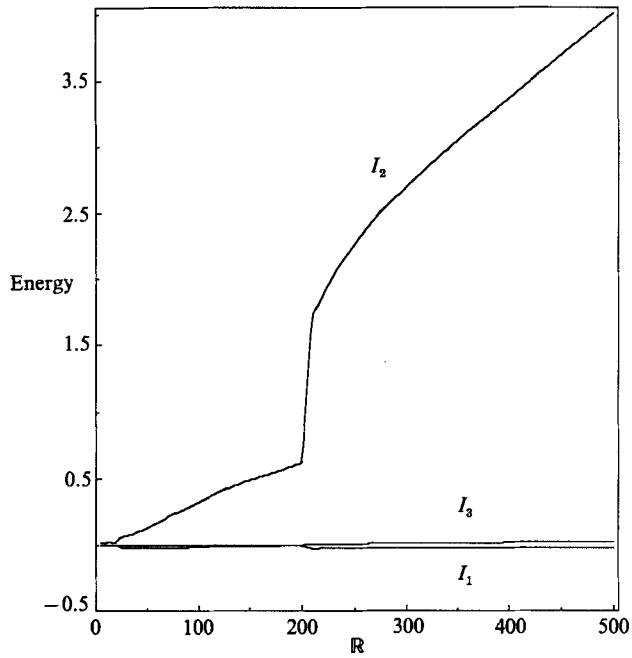

FIGURE 20. Variation with $\mathbb{R}$ of the energy of Reynolds stresses I_1 in the oil core, I_2 in the water annulus and I_3 in the oil layer on the wall, $I = I_1+I_2+I_3$, $(J^*, m, \eta, b) = (10^3, 0.1, 0.8, 0.9)$.

$1/m$ times larger than W' in the oil core, leading to larger Reynolds stress in water than in oil. Figure 20 shows that the dominant instability at high $\mathbb{R}$ continues to be associated with the Reynolds stress in the water annulus even when there is an oil layer at the wall; the Reynolds stress contribution I_2 in the intermediate low-viscosity layer is clearly much larger than the Reynolds stress contribution I_1 in oil core or I_3 in the oil layer on the pipe wall. The origin of this instability in the water when a layer of oil is on the wall needs clarification.

10.4. *Amplitude ratio and phase shift of the inner and outer interfaces*

We recall that $\delta_1(z,t)$ is the deviation of the inner interface from a mean radius R_1 and $\delta_2(z,t)$ is the deviation of the outer interface from a mean radius R_2. In the linearized theory

$$[\delta_1(z,t);\delta_2(z,t)] = \exp[\mathrm{i}\beta(z-ct)][\delta_1;\delta_2],$$

where $\delta_1 = |\delta_1|\,\mathrm{e}^{\mathrm{i}\phi_1}, \delta_2 = |\delta_2|\,\mathrm{e}^{\mathrm{i}\phi_2}$ are complex constants. The amplitude ratio $|\delta_1|/|\delta_2|$ and phase shift $\phi_2-\phi_1$ give the relative shape of the two interfaces in the linearized approximation.

In figure 21, we have plotted the amplitude ratio and phase shift as a function of $\mathbb{R}$ for $(J^*, m, \eta) = (10^3, 0.1, 0.8)$ and $b = 0.99$. There are three distinct regions of Reynolds numbers. In the first and third region, the flow of the corresponding two-layer problem is unstable. This means that the main instability for low and high $\mathbb{R}$ in three-layer flow is associated with the core–lubricant interface or the water annulus. The magnitude of the amplitude ratio for these $\mathbb{R}$ is largely dependent on the thickness $1-b$ of the outer layer. The instability in these cases is reflected in the relatively large deformation of the inner interface. For $\mathbb{R}$ in the range $\mathbb{R}_{\mathrm{L}} < \mathbb{R} < \mathbb{R}_{\mathrm{U}}$, the two-layer core–annular flow is stable and the only instability is due to interfacial friction at the outer interface and $|\delta_1|/|\delta_2| < 1$, with only small variations with the

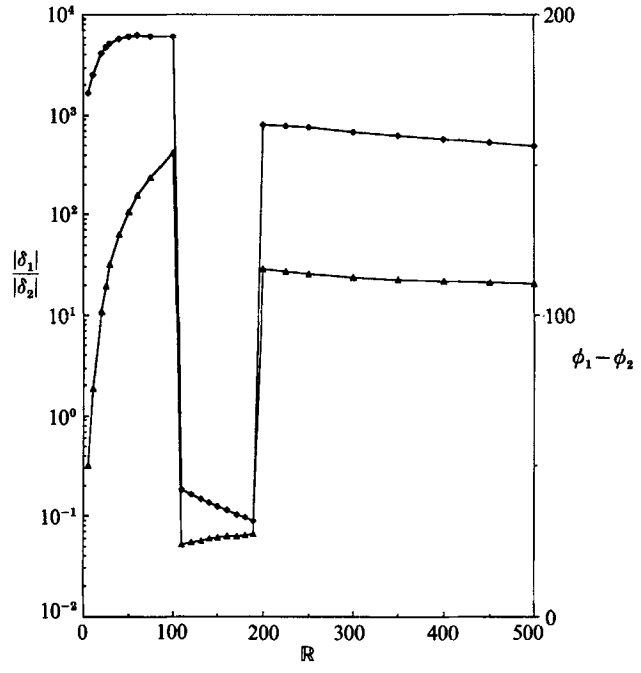

FIGURE 21. Amplitude ratio $|\delta_1|/|\delta_2|$ (◆), and phase shift $\phi_1-\phi_2$ (△) of the inner interface is larger. $(J^*, m, \eta, b) = (10^3, 0.1, 0.8, 0.99)$.

thickness $1-b$. There is always a phase shift between the two interfaces, except at the smallest $\mathbb{R}$ where interfacial tension is dominant. The phase shifts and amplitude ratios appear to tend to limiting values for large $\mathbb{R}$.

11. Conclusions

Linear stability analysis of core–annular flow leads to the following conclusions:

(1) There are three different kinds of instability identified through the energy analysis: (*a*) an interfacial tension instability or capillary instability; (*b*) an interfacial friction instability due to the viscosity difference across the interface; (*c*) a Reynolds stress instability.

(2) For all cases, at the lowest Reynolds number instability due to interfacial tension is dominant.

(3) Interfacial friction causes instability in two-layer flow with $m > 1$ when $\mathbb{R}$ is large and the water core is not very thin. It may also dominate the instability of three-layer flow at values of $\mathbb{R}$ in the range where two-layer core–annular flow with $m < 1$ would be stable if the water fraction was smaller.

(4) Instability due to the Reynolds stress is dominant in two-layer flow with $m < 1$ and in three-layer flow when $\mathbb{R}$ is sufficiently large (corresponding to the upper branch of the neutral curve) and the core is not very thin.

(5) The Reynolds stress instability is always associated with the less-viscous fluid layer. Even in the three-layer flow where a viscous layer of fluid is on the pipe wall, the Reynolds stress instability is induced by the less-viscous fluid in the intermediate layer. The possibility raised by the work of Hooper & Boyd (1987) that this instability is due to the disturbance vorticity generated by the solid boundary needs

to be reconciled with the observation that we have this type of instability in the water even when it does not touch the solid boundary.

(6) Comparison with the experiments of Charles *et al.* (1961) suggests that bubbles or slugs of oil in water are associated with interfacial tension instability or capillary instability, the emulsification of water into oil is correlated with the Reynolds stress instability. The water fraction seems to be an important factor in determining the phase inversion, with water emulsions or stable core–annular flow for small water fraction and some form of oil bubbles in water for larger water fractions. And comparison with the experiments of Olbricht & Aul also suggests that interfacial friction instability generates interfacial waves which may equilibrate nonlinearily.

(7) Two-layer core–annular flow with $m < 1$ and η near 1 undergoes different instabilities as $\mathbb{R}$ is increased: instability due to interfacial tension; stabilization of the instability of interfacial tension associated with the growth of instability due to interfacial friction; complete stabilization of core–annual flow; instability due to the growth of Reynolds stresses in the lubricating layer. If η is smaller than say 0.7, the stabilization of core–annular flow will not occur. When the core is very small, $\eta \to 0$ only instability, due to interfacial tension (capillary instability), will occur.

(8) Two-layer flow with $m > 1$ is always unstable. It is only weakly unstable if the thickness of the oil coating is very small (the maximum growth rate $\tilde{\sigma} \to 0$ as $\eta \to 1$).

(9) In two-layer flow with $m > 1$, there are two instabilities: interfacial tension at lower $\mathbb{R}$; interfacial friction at higher $\mathbb{R}$. Instability due to Reynolds stresses does not occur, one fluid is always stable against small disturbances.

(10) Core–annular flow with a very thin core ($\eta \to 0$) undergoes instability due to interfacial tension alone, when $m > 1$ or $m < 1$. The disturbance energies associated with the Reynolds stress minus dissipation, $I-D$, and with interfacial friction B_2 are stabilizing. The neutral curves and wavenumbers of the fastest growing wave are independent of $\mathbb{R}$; the maximum growth rate is proportional to $1/\mathbb{R}$. This is consistent with the fact that as $\eta \to 0$, the relevant eigenvalue $\tilde{c} = R(1-c)$ is independent of $\mathbb{R}$, as in the theory of capillary instability.

(11) In general, the capillary instability of jets depends on parameters J^*, m and ζ. Rayleigh's capillary instability of an inviscid jet with $\tilde{\alpha} = 0.697$ emerges when the density ratio ζ and viscosity ratio m are very small. Capillary instability of a 'hollow jet' with $\tilde{\alpha} = 0.484$ emerges when the density ratio ζ and viscosity ratio m are very large.

(12) Three-layer core–annular flow (1) can be regarded as the composition of one two-layer flow with $m < 1$ (2) and another two-layer flow with $m > 1$ (3). The neutral curve for (1) can be viewed as a combination of the neutral curve for (3) and the deformed neutral curve for (2) in which the upper branch is moved to larger wavenumbers.

(13) Three-layer flow is always unstable. Roughly speaking, as $\mathbb{R}$ increases, it undergoes the same sequence of instabilities as two-layer flow with $m < 1$ except that the stable core–annular flow region is destabilized by interfacial friction at the outer interface.

(14) As the viscous layer coating the pipe wall becomes thinner ($b \to 1$), the difference between two-layer flow with $m < 1$ and three-layer flow tends to zero. Thus, a thin layer of oil on the wall of a pipe need not be an impediment to lubricated pipelining.

(15) The amplitude ratio $|\delta_1|/|\delta_2|$ is largely dependent on the thickness of the outer layer $(1-b)$, when the instability is induced at the inner interface or in the middle

water annulus reflecting a relatively large deformation of the inner interface. Except at the smallest $\mathbb{R}$, there is always a phase shift between two interfaces.

Joseph, Nguyen & Beavers (1984) addressed the problem of non-uniqueness of the flow of two immiscible fluids, and they exhibited different situations in which different flows could be found for the same prescription of data. The study of linear stability does reduce the number of flows that could be observed, but does not restore uniqueness. For the present problem, we would like, for example, to determine if the flows that arise in experiments like those of Charles *et al.* (1961) are finally uniquely determined by data, or if they depend on initial conditions. If we fix the total volume flux of the two fluids, and the water fraction, we could create a continuum of configurations for initial conditions; the water could be initially on the wall, or in the centre, in annular rings, in drops of various sizes. We do not yet know if a single flow, where single is defined in a suitable statistical sense, would emerge from all these conditions.

This work was supported by the Department of Energy; the National Science Foundation, Fluid Mechanics and the Army Research Office, Mathematics. Computer results were obtained under a grant from the academic Computing Services and Systems of the University of Minnesota.

REFERENCES

BLENNERHASSETT, P. J. 1980 On the generation of waves by wind. *Proc. R. Soc. Lond.* A **298**, 451–494.

CHANDRASEKHAR, S. 1961 *Hydrodynamics and Hydromagnetic Stability*. Dover.

CHARLES, M. E., GOVIER, G. W. & HODGSON, G. W. 1961 The horizontal pipeline flow of equal density oil-water mixtures. *Can. J. Chem. Engng* **39**, 17–36.

FRENKEL, A. L., BABCHIN, A. J., LEVICH, B. G., SHLANG, T. & SHIVASHINSKY, G. I. 1987 Annular flows can keep unstable films from breakup: Nonlinear saturation of capillary instability. *J. Colloid Interface Sci.* **115**, 225–233.

GALDI, M. 1987 Energy instability in fluid dynamics. In *Energy Stability and Convection* (ed. P. Galdi & B. Straughn). Research Notes in Mathematics. Longman.

HASSON, D., MANN, U. & NIR, A. 1970 Annular flow of two immiscible liquids, I. Mechanisms. *Can. J. Chem. Engng* **48**, 514–520.

HASSON, D. & NIR, A. 1970 Annular flow of two immiscible liquids, II. Analysis of core-liquid ascent. *Can. J. Chem. Engng* **48**, 521–525.

HICKOX, C. E. 1971 Instability due to viscosity and density stratification in axisymmetric pipe flow. *Phys. Fluids* **14**, 251–262.

HOOPER, A. 1987 A note on the energy stability equation for Couette flow of two superposed viscous fluids. In *Energy Stability and Convection* (ed. P. Galdi & B. Straughn). Research Notes in Mathematics. Longman.

HOOPER, A. & BOYD, W. G. 1983 Shear flow instability at the interface between two viscous fluids. *J. Fluid Mech.* **128**, 507–528.

HOOPER, A. & BOYD, W. G. 1987 Shear flow instability due to a wall and a viscosity discontinuity at the interface. *J. Fluid Mech.* **179**, 201–225.

JOSEPH, D. D. 1987 Two fluids heated from below. In *Energy Stability and Convection* (ed. P. Galdi & B. Straughn). Research Notes in Mathematics. Longman.

JOSEPH, D. D., NGUYEN, K. & BEAVERS, G. 1984 Non-uniqueness and stability of the configuration of flow of immiscible fluids with different viscosities. *J. Fluid Mech.* **141**, 319–345.

JOSEPH, D. D., RENARDY, M. & RENARDY, Y. 1983 Instability of the flow of immiscible liquids with different viscosities in a pipe. *Math. Res. Center Tech. Summary Rep. 2503.*

JOSEPH, D. D., RENARDY, Y. & RENARDY, M. 1984 Instability of the flow of immiscible liquids with different viscosities in a pipe. *J. Fluid Mech.* **141**, 319–345.

OLIEMANS, R. V. A. 1986 *The Lubricating Film Model For Core–Annular Flow*. Delft University Press.

OLIEMANS, R. V. A. & OOMS, G. 1986 Core–annular flow of oil and water through a pipeline. In *Multiphase Science and Technology*, Vol. 2 (ed. G. F. Hewitt, J. M. Delhaye & N. Zuber). Hemisphere.

PREZIOSI, L., CHEN, K. & JOSEPH, D. D. 1989 Lubricated pipelining: stability of core–annular flow (referred to as PCJ). *J. Fluid Mech.* **201**, 323–356.

RENARDY, M. & JOSEPH, D. D. 1986 Hopf bifurcation in two-component flow. *SIAM J. Math. Anal.* **17**, 894–910.

RENARDY, Y. 1985 Instability at the interface between two shearing fluids in a channel. *Phys. Fluids* **28**, 3441–3443.